

Is the Information Bottleneck Robust Enough? Towards Label-Noise Resistant Information Bottleneck Learning

Yi Huang¹, Qingyun Sun^{1*}, Yisen Gao², Haonan Yuan¹, Xingcheng Fu³, Jianxin Li¹

¹SKLCCSE, School of Computer Science and Engineering, Beihang University, Beijing, China

²Department of Computer Science and Engineering, HKUST, Hong Kong, China

³Key Lab of Education Blockchain and Intelligent Technology, Ministry of Education, Guangxi Normal University, China
 {yihuang, sunqy, yuanhn, lijx}@buaa.edu.cn, ygaodi@cse.ust.hk, fuxc@gxnu.edu.cn

Abstract

The Information Bottleneck (IB) principle facilitates effective representation learning by preserving label-relevant information while compressing irrelevant information. However, its strong reliance on accurate labels makes it inherently vulnerable to label noise, prevalent in real-world scenarios, resulting in significant performance degradation and overfitting. To address this issue, we propose **LaT-IB**, a novel *Label-Noise Resistant Information Bottleneck* method which introduces a “Minimal-Sufficient-Clean” (MSC) criterion. Instantiated as a mutual information regularizer to retain task-relevant information while discarding noise, MSC addresses standard IB’s vulnerability to noisy label supervision. To achieve this, LaT-IB employs a noise-aware latent disentanglement that decomposes the latent representation into components aligned with the clean label space and the noise space. Theoretically, we first derive mutual information bounds for each component of our objective including prediction, compression, and disentanglement, and moreover prove that optimizing it encourages representations invariant to input noise and separates clean and noisy label information. Furthermore, we design a three-phase training framework: Warmup, Knowledge Injection and Robust Training, to progressively guide the model toward noise-resistant representations. Extensive experiments demonstrate that LaT-IB achieves superior robustness and efficiency under label noise, significantly enhancing robustness and applicability in real-world scenarios with label noise.

1 Introduction

The Information Bottleneck (IB) principle (Tishby, Pereira, and Bialek 2000) provides a fundamental theoretical framework for balancing compression and relevance in representation learning. Rooted in information theory, it has increasingly influenced the development of deep learning (Hu et al. 2024). IB encourages representations Z that retain only task-relevant information while discarding irrelevant or redundant input features using Mutual Information (MI) $I(\cdot; \cdot)$:

$$\min -I(Y; Z) + \beta I(X; Z). \quad (1)$$

IB-based methods aim to extract “Minimal-Sufficient” representations, inherently filtering out input noise and spurious correlations. This selective encoding mechanism contributes

CIFAR10	40% asym noise	50% sym noise
ResNet34	77.78%	79.4%
VIB ($\beta = 0.01$)	73.80%	10.0%
Cora (40% noise)	Epoch: 0 → 20	Epoch: 20 → 100
GIB	22.9% → 69.5% steady increase ↑	69.5% → 55.1% steady decline ↓

Table 1: Performance of IB methods under noise conditions.

to their notable robustness under noisy or adversarial input perturbations (Shamir, Sabato, and Tishby 2010).

However, input noise rarely eliminates all useful information, allowing IB to extract meaningful features from Y . In contrast, label noise corrupts the supervisory signal, causing $I(Y; Z)$ to mislead Z to fit incorrect labels, thereby reducing robustness. This vulnerability is critical in real-world settings, where label noise is common and can severely harm performance, as real graphs are often disturbed by noise and unexpected factors. (Li et al. 2025). To address this, Label-Noise Representation Learning (LNRL) (Song et al. 2022) aims to extract robust features despite label corruption.

To empirically test the hypothesis that **IB is inherently vulnerable to label noise**, we conduct preliminary experiments on two tasks: image classification in computer vision and node classification in graph learning. We evaluate two representative IB-based methods: VIB (Alemi et al. 2017) and GIB (Wu et al. 2020). As shown in Table 1, VIB suffers performance drops and even training collapse, while GIB exhibits degraded accuracy. See Appendix E.3 for details.

To mitigate this, a simple remedy is to denoise the labels prior to applying IB. However, this two-stage pipeline is inherently suboptimal in both theory and practice.

Theorem 1.1 (Cumulative Degradation). *In the two-stage approach, f_1 is used to modify the labels $Y' = f_1(\mathcal{D})$, and f_2 is responsible for extracting valid information from \mathcal{D} while approximating the prediction result to $f_1(\mathcal{D})$. For one-stage model $g(\mathcal{D})$, it extracts the relevant information while removing noise. If the denoising abilities of f_1 and g are the same, the following inequality holds:*

$$P(f_2(\mathcal{D}) \neq g(\mathcal{D})) \geq \frac{H(Y'|\mathcal{D}) - 1}{\log(|\mathcal{Y}| - 1)}, \quad (2)$$

*Corresponding Author

Copyright © 2026, Association for the Advancement of Artificial Intelligence (www.aaai.org). All rights reserved.

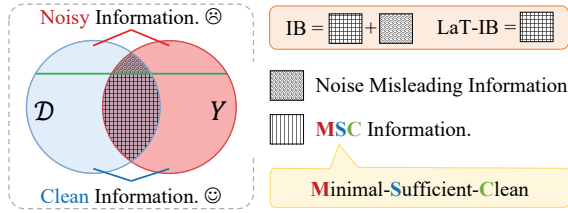


Figure 1: Comparison between LaT-IB and IB Principle.

where \mathcal{Y} denotes the support of Y , and $|\mathcal{Y}|$ denotes the number of elements in \mathcal{Y} . The two models perform identically iff f_2 achieves the error lower bound and $H(Y'|\mathcal{D}) = 0$.

The proof of Theorem 1.1 is given in Appendix C.1. It demonstrates that cascading a denoising model f_1 with an IB learner f_2 leads to cumulative information loss compared with a unified model g , due to the extended information path. This phenomenon is further validated by empirical results, which show a clear degradation in the denoising effect when models are cascaded. See Appendix E.3 for detailed results.

Core Issue: How can the IB principle be effectively applied to real-world scenarios with complex and unknown label noise, in order to learn representations that are both “Minimal-Sufficient” and robust to noisy supervision?

Due to unknown label noise and the difficulty of integrating denoising with Information Bottleneck, applying IB in practice requires confronting the following key challenges:

- How to formulate the IB objective under label noise to learn clean representation. (▷ Section 4.1)
- How to optimize MI under label noise that distorts task-relevant representation learning. (▷ Section 4.2)
- How to effectively disentangle clean and noisy representations without knowing noisy samples. (▷ Section 4.3)

Present work. To address the core issue and tackle the key challenges, we propose a **Label-Noise Resistant Information Bottleneck (LaT-IB)** method. Centered on the idea of disentangling representations into clean and noisy label spaces, we formulate an IB training objective tailored for noisy supervision and theoretically justify its effectiveness through upper and lower bound analysis. To this end, we design a three-phase training framework: Warmup, Knowledge Injection and Robust Training, which gradually guides the model to learn “Minimal-Sufficient-Clean” (MSC) representations. A comparison between LaT-IB and standard IB principle is illustrated in Figure 1. Our contributions are:

- We identify the inherent vulnerability of IB to label noise and prove that denoising before IB is suboptimal.
- We propose a LaT-IB method that introduces MSC criterion of representations to enhance IB’s robustness to label noise while maintaining its essential characteristics.
- We provide theoretical upper and lower bounds for LaT-IB, showing how disentangling clean and noise features enables robust representation learning. Based on this, we design a principled model and training framework.
- Extensive experiments evaluate LaT-IB’s robustness and efficiency, outperforming baselines under label noise and adversarial attacks across diverse tasks and domains.

2 Related Work

2.1 Information Bottleneck for Robustness

The IB (Tishby, Pereira, and Bialek 2000) framework introduces a feature learning paradigm grounded in information theory. Works such as VIB (Alemi et al. 2017) and GIB (Wu et al. 2020) have advanced its practical use. Considering robustness, methods like DisenIB (Pan et al. 2021) and DGIB (Yuan et al. 2024) show reasonable robustness to input features, with studies (Xie et al. 2023; Pensia, Jog, and Loh 2020) further improving resilience to input noise.

Considering the presence of label noise, RGIB (Zhou et al. 2023) explores structural noise in GNNs to improve link prediction robustness. However, comprehensive studies on the vulnerability of IB to label noise still remain lacking.

2.2 Label-Noise Representation Learning

The LNRL aims to improve model robustness and representation quality under noisy label conditions. Existing approaches for learning with noisy labels include sample selection (Patel and Sastry 2023; Wei et al. 2020), which filters out likely noisy samples; robust loss functions (Zhang and Sabuncu 2018; Wang et al. 2019), which modify loss terms to reduce sensitivity to incorrect labels; noise-robust architectures (Liu et al. 2020), which use regularization to avoid overfitting noise; and data augmentation, such as mixup-based methods (Zhang et al. 2018; Harris et al. 2020), which interpolates samples to improve generalization.

However, most methods ignore representation-level constraints, making it hard to learn task-relevant and noise-invariant features under severe noise or distribution shifts.

3 Preliminary Analysis

Notation. We primarily define the input data \mathcal{D} . For vision tasks, $\mathcal{D} = X$, where $X \in \mathbb{R}^{N \times C \times P \times Q}$ denotes N samples with C channels and spatial size $P \times Q$ (e.g., height \times width). For graph learning tasks, $\mathcal{D} = \mathcal{G} = (X, A)$, where $X \in \mathbb{R}^{N \times d}$ denotes d -dimensional features for N nodes and $A \in \mathbb{R}^{N \times N}$ represents the adjacency matrix. Each sample $\xi_i \in \mathcal{D}$ has a label $y_i \in \mathcal{Y}$, which may be corrupted by noise during the labeling process. We denote Y_c and Y_n as the clean and noisy counterparts of Y respectively.

Analysis of IB Theory with Label Noise. In the traditional IB, $I(X; Z)$ encourages minimal representations by compressing the input, while $I(Y; Z)$ ensures sufficiency by preserving task-relevant information. However, when the label Y is corrupted by noise, maximizing $I(Y; Z)$ is equivalent to maximizing $I(Y_c, Y_n; Z)$, which inadvertently causes the learned representation Z to capture noise Y_n , thus compromising robustness and degrading performance.

In this study, we aim to mitigate the negative impact of label noise on model performance while preserving the “Minimal-Sufficient” property of the IB method. Ideally, we consider a robust IB method \mathcal{M}_{IB} that, given a dataset (\mathcal{D}, Y) where Y consists of both clean labels $y_i \in Y_c$ and noisy labels $y_j \in Y_n$, aims to satisfy the following objective:

$$\begin{aligned} & \min -I(Z; Y_c) + \beta I(Z; \mathcal{D}) \\ & \text{s.t. } Z = \mathcal{M}_{IB}(\mathcal{D}, Y). \end{aligned} \quad (3)$$

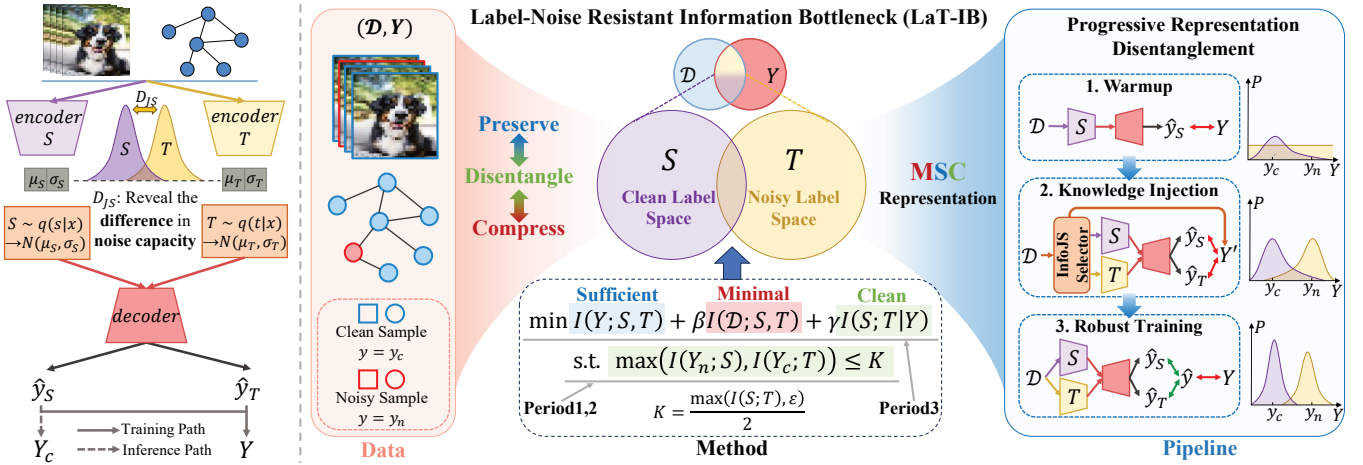


Figure 2: Left: The overall LaT-IB model architecture with dual encoders for extracting features from clean (S) and noisy (T) label spaces, and a shared decoder. Right: An illustration of the LaT-IB method, which disentangles representations to extract “Minimal-Sufficient-Clean” features. Specifically, its pipeline consists of three period: Warmup, Knowledge Injection and Robust Training, which transform Eq. (8) from a theoretical formulation into a practical training procedure.

Compared to the traditional IB objective, the goal of Eq. (3) is to maximize the MI between the learned representation and the clean labels Y_c , rather than with all observed labels Y . However, **whether each label is clean or noisy is unknown**. In the next section, we introduce a concrete solution to mitigate IB’s vulnerability to label noise.

4 Methodology

In this paper, we propose Label-Noise Resistant Information Bottleneck (LaT-IB), along with theoretical formulation, model architecture and a tailored training framework, as illustrated in Figure 2. We begin by presenting the formal objective of LaT-IB and interpreting its theoretical implications. To enable efficient optimization, we derive upper and lower bounds that simplify the objective, effectively bridging the gap between theory and practice. Finally, drawing on key insights, we design a three-phase training framework: Warmup, Knowledge Injection and Robust Training, clarify the role of each phase and facilitate the progressive disentanglement of clean and noise-related representations.

4.1 Label-Noise Resistant Information Bottleneck

In real-world datasets, each training sample may have either a clean or a corrupted label, and sometimes both possibilities coexist probabilistically. Using a unified representation for all samples under such ambiguity can cause conflicting features and hurt downstream tasks. To mitigate this, we disentangle the representation into two parts: S under the clean label space, and T under the noise space. Under this disentanglement, the objective in Eq. (3) can be reformulated as:

$$\min -I(S; Y_c) + I(\mathcal{D}; S, T). \quad (4)$$

Since only Y are available in the dataset, we implicitly associate it with the joint representation of S and T , where disentanglement is encouraged by $\min I(S; T|Y)$. A successful disentanglement implies that S and T encode conditionally

independent given Y , capturing distinct semantics. With β and γ as balancing factors, the LaT-IB is formulated as:

$$\min \underbrace{-I(Y; S, T)}_{\text{prediction term}} + \beta \underbrace{I(\mathcal{D}; S, T)}_{\text{compression term}} + \gamma \underbrace{I(S; T|Y)}_{\text{disentanglement term}}, \quad (5)$$

However, Eq. (5) still cannot map S to clean features and T to noise features. To address this and further explore its representational meaning, we introduce two lemmas below.

Lemma 4.1 (Nuisance Invariance). *Taking the part of \mathcal{D} that does not contribute to Y as \mathcal{D}_n (\mathcal{D}_n is independent of Y), and considering the Markov chain $(Y, \mathcal{D}_n) \rightarrow \mathcal{D} \rightarrow (S, T)$, the following inequality holds:*

$$I(\mathcal{D}_n; S, T) \leq -I(Y; S, T) + I(\mathcal{D}; S, T). \quad (6)$$

Lemma 4.2 (Feature Convergence). *Assuming that Y can potentially contain all information about Y_c and Y_n , the following inequality holds when $\max(I(Y_n; S), I(Y_c; T)) \leq \max(I(S; T), \varepsilon)/2 = K, \varepsilon > 0, \varepsilon \in \mathbb{R}$ is satisfied:*

$$-I(Y_c; S) - I(Y_n; T) - \varepsilon \leq -I(Y; S, T) + I(S; T|Y). \quad (7)$$

The detailed proofs of these lemmas can be found in Appendix C.2. Lemma 4.1 demonstrates that optimizing $\min -I(Y; S, T) + I(\mathcal{D}; S, T)$ in Eq. (5) ($\beta = 1$) essentially reduces the model’s tendency to learn features irrelevant to Y (denoted as \mathcal{D}_n). Lemma 4.2 further indicates that, when the MI terms $I(Y_n; S)$ and $I(Y_c; T)$ are sufficiently small, optimizing $\min -I(Y; S, T) + I(S, T|Y)$ in Eq. (5) ($\gamma = 1$) effectively strengthens the mapping relationships $S \rightarrow Y_c$ and $T \rightarrow Y_n$. Based on these insights, we can first ensure the conditions in Lemma 4.2 then optimize the main objective in Eq. (5) as a form of **progressive representation disentanglement**. This enables the model to separate clean and noisy features while avoiding learning irrelevant noise \mathcal{D}_n .

By combining Lemma 4.1 and Lemma 4.2, we obtain a principled training objective that integrates sufficiency, com-

pression, and clean-noise disentanglement:

$$\begin{aligned} & \min -\underbrace{I(Y; S, T)}_{\text{Sufficient}} + \beta \underbrace{I(\mathcal{D}; S, T)}_{\text{Minimal}} + \gamma \underbrace{I(S; T|Y)}_{\text{Clean}} \\ & \text{s.t. } \underbrace{\max(I(Y_n; S), I(Y_c; T))}_{\text{Clean}} \leq K. \end{aligned} \quad (8)$$

4.2 Bound Analysis and Implementation

Building on the formulation introduced in the previous section, we now turn to the optimization of the proposed objective in Eq. (8). Since directly optimizing the multivariate MI is intractable, we first simplify the original objective by analyzing upper and lower bounds of MI, and then present the implementation strategy for each term. All proposition proofs are provided in the Appendix C.3.

Proposition 4.1 (The upper bound of $-I(Y; S, T)$). *Given the label Y and the variable S, T that learns the characteristics of the clean label space and the noisy label space respectively, we have:*

$$-I(Y; S, T) \leq -\max(I(Y; S), I(Y; T)). \quad (9)$$

Intuitively, Eq. (9) encourages encoders to focus on learning its own knowledge, ensuring consistency in the learned representation. Further, since MI terms are intractable, each $I(Y; Z)$ with $Z \in \{S, T\}$ is lower-bounded by the cross-entropy loss using a variational approximation $q_\theta(y|z)$:

$$I(Y; Z) \geq \mathbb{E}_{p(y, z)} (\log(q_\theta(y|z))) := -\mathcal{L}_{CE}(Z, Y), \quad (10)$$

Proposition 4.2 (The upper bound of $I(\mathcal{D}; S, T)$). *Let \mathcal{D}, S, T be random variables. Assume the probabilistic mapping $p(\mathcal{D}, S, T)$ follows the Markov chain $S \leftrightarrow \mathcal{D} \leftrightarrow T$. Then:*

$$I(\mathcal{D}; S, T) \leq I(\mathcal{D}; S) + I(\mathcal{D}; T). \quad (11)$$

The implementation of each term $I(\mathcal{D}; \cdot)$ remains consistent with that in VIB (Alemi et al. 2017) and GIB (Wu et al. 2020), achieved by minimizing the KL divergence between the variational posterior $q(\cdot|\mathcal{D})$ and the prior $p(\cdot)$.

Proposition 4.3 (Reformulation of $I(S, T|Y)$). *Given the label Y and the variable S, T , minimizing $I(S, T|Y)$ is equivalent to minimize $I(S, Y; T, Y)$.*

The Proposition 4.3 achieves the tractable transformation of conditional MI theoretically. However, minimizing the term $I(S, Y; T, Y) = D_{KL}[q(S, T, Y)||q(S, Y)q(T, Y)]$ is intractable since both distributions involve mixtures with many components. Therefore, we use the density-ratio trick (Sugiyama, Suzuki, and Kanamori 2012) by introducing a discriminator d , that learns to distinguish between samples from the joint distribution $q(s, t, y)$ and those from the product of marginals $q(s, y)q(t, y)$. In particular, we sample negative pairs $((s, y), (t, y'))$ from $q(s, y)q(t, y)$, where (s, y) and (t, y') are drawn independently, and positive pairs $((s, y), (t, y))$ from the joint distribution $q(s, t, y)$, where both s and t correspond to the same sample. The discriminator $d((s, y), (t, y'))$ is trained to output the probability that a given pair comes from the joint distribution, and the objective is to minimize the MI by solving the following problem:

$$\begin{aligned} & \min \max_q \max_d \mathbb{E}_{q(s, y)q(t, y)} \log d((s, y), (t, y')) \\ & + \mathbb{E}_{q(s, t, y)} \log(1 - d((s, y), (t, y))). \end{aligned} \quad (12)$$

When the discriminator cannot distinguish between joint and independent samples, the MI is effectively minimized.

Proposition 4.4 (Reformulation of the condition in Eq. (8)): $\max(I(Y_n; S), I(Y_c; T)) \leq K$. *Minimizing $I(Y_c; T)$ and $I(Y_n; S)$ is equivalent to maximize $I(Y_n; T)$ and $I(Y_c; S)$.*

Proposition 4.4 relaxes the condition in Eq. (8). Since the original MI calculation is mismatched and thus intractable, the relaxed formulation provides a tractable alternative that can be optimized efficiently, as described in Eq. (10).

4.3 Principle to Practice: LaT-IB Framework

Based on the theoretical analysis above, this section introduces the practical implementation of LaT-IB. To optimize the objective in Eq. (8), we adopt a three-phase training framework to **progressively disentangle the representation**. Specifically, we first introduce a **Warmup** period to provide the model with initial discriminative ability. Building on this, a **Knowledge Injection** period enforces the constraint by applying InfoJS selector, guiding the learning of encoder_{S/T} via selected samples. Finally the **Robust Training** period focuses on optimizing the complete objective with prior knowledge, refining the model's robustness.

Feature-Decomposed Dual Encoder Architecture Design. Based on the Observation 4.1, we adopt the Jensen-Shannon (JS) divergence as a metric to evaluate the noise retention capacity of the two encoders.

Observation 4.1. *With the decoder kept fixed, we train the encoder using datasets that share the same input X but differ in the level of label noise in Y . As the noise gap between the two datasets increases, the divergence between the resulting encodings from the encoder also becomes larger.*

Accordingly, Figure 2 illustrates the overall architecture of the LaT-IB: the model is designed with a dual-encoder, single-decoder framework, where the two encoders extract features S and T , respectively. Each encoder maps the input features to a high-dimensional Gaussian distribution, and the embeddings are sampled using the reparameterization trick.

Phase 1: Warmup with Discriminative Learning under Noise. To address the problem of noise memorization during training, we introduce a Warmup phase where the model **builds basic discriminative ability**. Specifically, we pre-train the clean encoder encoder_S using the full dataset, providing a foundation for more effective separation of clean and noisy samples in subsequent stages. The loss function in Warmup period is defined based on prediction \hat{y}_S :

$$\mathcal{L}_{Warmup} = \mathcal{L}_{CE}(\text{decoder}(S), Y) = \mathcal{L}_{CE}(\hat{y}_S, y). \quad (13)$$

Noise-Aware Sample Selection. Since the variables Y_c and Y_n are unobservable, we approximate the constraint $\max(I(Y_n; S), I(Y_c; T)) \leq K$ in Eq. (8) by selecting a partial set of confident samples to act as proxies for clean and noisy labels. Samples are then grouped into three categories for training: **Clean Set, Noise Set, and Uncertain Set**.

Observation 4.2. *For two different encoders, samples with more consistent predictions after passing through the decoder tend to have smaller divergence between their embeddings. In contrast, samples with inconsistent predictions correspond to larger embedding divergence.*

Observation 4.2 suggests that the divergence between encoders can be used to identify clean samples. Moreover, prior studies (Arpit et al. 2017; Song et al. 2019) have shown that models tend to fit clean samples earlier. Based on these insights, we designed the **InfoJS selector** as detailed in Algorithm B.2, which identifies clean (noisy) samples as those with MI between S and Y being in the top $\delta\%$ (bottom $\delta\%$) and JS divergence between S and T in the bottom $\delta\%$ (top $\delta\%$), respectively. Unselected samples are treated as the uncertain set. Labels are assigned as follows: $y' = y$ for Clean and Noise Sets, and $y' = g(\hat{y}_S)/g(\hat{y}_T)$ for Uncertain Set when training the encoder $_{S/T}$, where g denotes either a debiasing function (Menon et al. 2020) or one-hot mapping.

However, the InfoJS selector performs selection based on relative feature scores. To improve the quality of each set, we further enrich the sample composition by incorporating predicted confidence scores as an absolute criterion.

Phase 2: Knowledge Injection to Disentangle Representations. Once the model has acquired basic discriminative ability, we proceed to optimize the objective in Eq. (8). Given the condition and its reformulated form:

$$\underbrace{\max(I(Y_n; S), I(Y_c; T)) \leq K}_{\text{The original constraint in Eq. (8)}} \Rightarrow \underbrace{\max(I(Y_n; T)), \max(I(Y_c; S))}_{\text{The reformulated constraint in Proposition 4.4}}, \quad (14)$$

to satisfy the constraint, we introduce a Knowledge Injection phase to encourage the encoder $_{S,T}$ to learn disentangled representations. Furthermore, to enforce difference in noise representation between the two encoders, we incorporate the JS divergence D_{JS} based on Observation 4.1:

$$\begin{cases} \mathcal{L}_{Clean} = \mathcal{L}_{CE}(\hat{y}_S, y') - D_{JS}(s \| t), \\ \mathcal{L}_{Uncertain} = \mathcal{L}_{CE}(\hat{y}_S, y') + \mathcal{L}_{CE}(\hat{y}_T, y') + D_{JS}(s \| t), \\ \mathcal{L}_{Noise} = \mathcal{L}_{CE}(\hat{y}_T, y') - D_{JS}(s \| t), \end{cases} \quad (15)$$

For Clean and Noise Sets, divergence is maximized to increase encoder discrepancy; and for the Uncertain set, divergence is minimized to guide T towards meaningful patterns. It is worth noting that the Uncertain set is much smaller, thus has limited influence on the encoders' training process.

Empirically, minimizing the $I(\mathcal{D}; S, T)$ helps to leading to a more robust encoding space. To progressively disentangle the representation and achieve a minimal representation, we introduce a regularization term $\mathcal{L}_{Minimal}$ that approximates the $\min I(\mathcal{D}; S, T)$ term base on Proposition 4.2, and incorporate it into the loss function during the Knowledge Injection period to learn a compact representation:

$$\mathcal{L}_{Injection} = \mathcal{L}_{Clean} + \mathcal{L}_{Uncertain} + \mathcal{L}_{Noise} + \mathcal{L}_{Minimal}. \quad (16)$$

This facilitates a smoother transition to the third Robust Training stage. The implementation details of $\mathcal{L}_{Minimal}$ are provided in the Appendix D.1.

Phase 3: Robust Training for Representation Consistency. The Warmup stage establishes initial discriminative ability, while Knowledge Injection realized constraint

to guide the model toward informative and reliable samples. To further disentangle and enhance representation robustness under label noise, this period focuses on optimizing the full objective in Eq. (5): $\min -I(Y; S, T) + I(\mathcal{D}; S, T) + I(S; T|Y)$, aiming to learn noise consistent representations.

Section 4.2 has introduced the implementation of each objective term. Among them we propose \mathcal{L}_{ConCE} to optimize the term $I(Y; S, T)$ based Eq. (9) and (10):

$$\mathcal{L}_{ConCE} \leftarrow \sum \min(\mathcal{L}_{CE}(\hat{y}_S, y), \mathcal{L}_{CE}(\hat{y}_T, y)), \quad (17)$$

encouraging consistency between encoders and clean/noisy labels. Detailed formulations are provided in Appendix B.1.

The loss function for the Robust Training period is:

$$\mathcal{L}_{Robust} = \frac{1}{|\mathcal{B}|} \sum_{i=1}^{\mathcal{B}} [\underbrace{\mathcal{L}_{ConCE}(\hat{y}_S, \hat{y}_T, y)}_{\text{Eq. (17)}} + \beta \underbrace{\mathcal{L}_{Minimal}}_{\text{Eq. (11)}} - \gamma \underbrace{\log d(s_i, y_i; t_i, y_i)}_{\text{Proposition 4.3, Eq. (12)}}, \quad (18)$$

where \mathcal{B} denotes a training batch. In addition, we alternately update the discriminator d based on Eq. (12), using a random permutation π to approximate the marginal distribution:

$$\mathcal{L}_d = \frac{1}{|\mathcal{B}|} \sum_{i=1}^{\mathcal{B}} -\log(1 - d(s_i, y_i; t_{\pi(i)}, y_{\pi(i)})) - \log d(s_i, y_i; t_i, y_i). \quad (19)$$

5 Experiment

In this section, we conduct extensive experiments to evaluate the robustness and efficiency of the LaT-IB under diverse tasks and various types of noise, including real-world and synthetic label noise, as well as adversarial perturbation.¹

5.1 Experimental Settings

Datasets. We evaluate the proposed LaT-IB method on multiple datasets. For image classification, we utilize the CIFAR (Wei et al. 2022), Animal-10N (Song, Kim, and Lee 2019) and CIFAR (Krizhevsky, Hinton et al. 2009) datasets. For node classification tasks, we evaluate on Cora, Citeseer, Pubmed (Sen et al. 2008), and DBLP (Pan et al. 2016). More descriptions about datasets are provided in Appendix E.1.

Baselines. We compare our LaT-IB with four categories, 16 baselines in two scenarios: ① Classic IB methods; ② IB with robust loss functions; ③ Improved IB variants; ④ Two-stage denoising + IB methods. They comprehensively evaluate our LaT-IB's performance from multiple perspectives.

Label Noise Settings. To evaluate the robustness of LaT-IB and baselines against label noise, we conduct experiments in both image and graph classification tasks. For image classification, we evaluate on both real-world noisy datasets and synthetic settings with symmetric and asymmetric label noise, simulated using custom transition matrices as described in (Xiao et al. 2023). For node classification, we follow the protocol in (Wang et al. 2024) to inject uniform and pairwise label noise into graph labels.

¹Code available at: <https://github.com/RingBDStack/LaT-IB>

Method	Model	CIFAR-10N					CIFAR-100N	Animal-10N
		aggre	rand1	rand2	rand3	worst	noisy100	
Classic IB	VIB	86.11 \pm 0.34	83.69 \pm 0.50	83.69 \pm 0.46	83.76 \pm 0.29	73.80 \pm 0.59	53.29 \pm 0.09	76.28 \pm 0.51
	NIB	85.21 \pm 0.44	84.03 \pm 1.43	81.98 \pm 0.68	82.39 \pm 0.43	73.51 \pm 0.82	48.11 \pm 0.40	75.62 \pm 0.64
Robust Loss	VIB (\mathcal{L}_{GCE})	85.70 \pm 0.08	84.32 \pm 0.50	83.97 \pm 0.38	84.25 \pm 0.68	78.88 \pm 0.27	—	81.72 \pm 1.77
	VIB (\mathcal{L}_{SCE})	83.95 \pm 0.10	82.65 \pm 0.25	82.84 \pm 0.31	82.50 \pm 0.24	73.81 \pm 1.54	50.71 \pm 0.14	77.17 \pm 0.44
Improved IB	SIB	89.99 \pm 0.08	84.75 \pm 1.04	85.07 \pm 0.72	85.39 \pm 0.50	70.58 \pm 0.50	50.82 \pm 0.41	83.95 \pm 0.14
	DT-JSCC	85.46 \pm 0.44	81.85 \pm 0.66	81.14 \pm 0.55	81.03 \pm 0.34	69.73 \pm 1.15	43.61 \pm 0.19	78.98 \pm 0.23
Denoise + IB	JoCoR+VIB	86.39 \pm 0.18	86.45 \pm 0.02	86.53 \pm 0.29	86.60 \pm 0.11	81.65 \pm 0.15	54.24 \pm 0.18	75.45 \pm 0.27
	(ELR+)+VIB	92.65 \pm 0.27	92.09 \pm 0.25	92.01 \pm 0.20	91.93 \pm 0.15	86.68 \pm 0.25	61.06 \pm 0.34	85.87 \pm 0.15
	Promix+VIB	92.35 \pm 0.38	92.59 \pm 0.40	92.42 \pm 0.17	92.54 \pm 0.21	91.24 \pm 0.28	63.91 \pm 0.19	85.47 \pm 0.51
Ours	LaT-IB	94.17 \pm 0.12	93.25 \pm 0.11	93.19 \pm 0.09	93.03 \pm 0.11	87.95 \pm 0.22	63.59 \pm 0.67	88.49 \pm 0.11

Table 2: Classification accuracy (%) on the CIFAR-10N/100N and Animal-10N dataset. All the best results are highlighted in **bold**, and the second-best results are underlined.

Method	Model	Clean	Uniform Noise				Pair Noise			
			10%	20%	30%	40%	10%	20%	30%	40%
Classic	GIB	71.57 \pm 1.18	<u>70.50</u> \pm 1.85	64.30 \pm 6.45	63.90 \pm 3.51	<u>62.67</u> \pm 1.35	68.67 \pm 3.47	61.30 \pm 14.57	67.53 \pm 4.77	55.57 \pm 14.33
Robust Loss	GIB (\mathcal{L}_{GCE})	69.93 \pm 0.69	67.43 \pm 3.21	61.67 \pm 7.19	47.80 \pm 18.62	43.47 \pm 14.50	50.93 \pm 0.52	55.33 \pm 11.23	62.37 \pm 6.99	36.90 \pm 15.23
	GIB (\mathcal{L}_{SCE})	72.53 \pm 0.12	70.17 \pm 2.10	<u>71.63</u> \pm 2.05	62.90 \pm 8.09	51.87 \pm 6.03	69.30 \pm 1.66	68.23 \pm 3.41	65.13 \pm 5.02	51.13 \pm 11.30
Improved IB	CurvGIB	64.63 \pm 5.28	65.67 \pm 5.85	54.67 \pm 10.09	54.00 \pm 2.41	54.97 \pm 2.78	59.97 \pm 9.00	62.07 \pm 5.15	66.63 \pm 1.94	54.57 \pm 1.25
	IS-GIB	71.00 \pm 1.22	69.97 \pm 1.41	64.30 \pm 2.30	<u>59.77</u> \pm 3.70	53.77 \pm 4.41	64.83 \pm 2.34	62.50 \pm 1.51	62.50 \pm 1.31	55.40 \pm 4.74
Denoise + IB	RNCGLN+GIB	70.57 \pm 0.99	69.50 \pm 0.86	63.43 \pm 5.90	62.83 \pm 4.15	53.27 \pm 14.47	69.90 \pm 1.69	68.20 \pm 2.14	66.47 \pm 3.21	56.77 \pm 15.11
	CGNN+GIB	71.87 \pm 1.99	68.97 \pm 3.09	65.47 \pm 4.77	<u>64.93</u> \pm 2.46	48.83 \pm 6.48	59.03 \pm 12.67	69.77 \pm 1.77	68.50 \pm 2.83	53.93 \pm 13.85
Ours	LaT-IB	74.97 \pm 0.68	74.90 \pm 2.09	73.40 \pm 2.62	70.50 \pm 3.86	72.20 \pm 4.22	75.63 \pm 0.46	73.03 \pm 1.77	70.07 \pm 3.20	68.77 \pm 2.29

Table 3: Classification accuracy (%) on the Pubmed dataset under different noise types and noise rates. All the best results are highlighted in **bold**, and the second-best results are underlined.

Adversarial Attack Settings. As discussed in Appendix D.1, the implementation of $I(\mathcal{D}; S, T)$ in our LaT-IB framework aligns with prior work VIB and GIB, thereby theoretically inheriting their robustness properties. To empirically verify this claim, we evaluate LaT-IB’s performance under adversarial perturbations in the image classification setting. Specifically, we adopt the FGSM (Goodfellow, Shlens, and Szegedy 2015) attack to perturb input images with $\epsilon \in \{0.05, 0.1, 0.2\}$, controlling the perturbation strength. Combined with noisy labels during training, this setup evaluate the robustness of model under compound noise conditions.

5.2 Robustness Against Label Noise

In this section, we evaluate the representation capability of our proposed method under various label noise conditions. Specifically, we investigate whether the LaT-IB model can effectively learn robust representations when trained on data corrupted by different types and levels of label noise.

Results. In most scenarios, our proposed LaT-IB method outperforms other baseline approaches as shown in Table 2 and 3. In certain cases, however, methods that first perform denoising and then apply IB achieve better results, likely due to the strong denoising capacity of those models. Nev-

ertheless, such two-stage methods involve longer training pipelines and are more vulnerable to adversarial attacks, as will be demonstrated in the next section. Additional experimental results on label noise are shown in Appendix E.

5.3 Robustness Against Adversarial Perturbations

In this section, to further validate the “Minimal-Sufficient” property in MSC of the proposed LaT-IB method, we apply perturbations to the input data \mathcal{D} . The perturbed data is then fed into models trained under noisy label settings. This setup enables a comprehensive evaluation of model robustness against diverse noise, including inputs and labels.

Results. The results demonstrate that the LaT-IB method exhibits strong robustness against adversarial attacks, significantly outperforming other approaches, as shown in Table 4. Notably, two-stage methods suffer a substantial performance drop under attack due to the increased number of vulnerable components, further highlighting their limitations.

5.4 Ablation Study

In this section, we analyze the effectiveness of different training stages in the LaT-IB framework. To investigate the

Model	CIFAR-10N (aggre)				CIFAR-10N (worst)			
	No attack	$\varepsilon = 0.05$	$\varepsilon = 0.1$	$\varepsilon = 0.2$	No attack	$\varepsilon = 0.05$	$\varepsilon = 0.1$	$\varepsilon = 0.2$
VIB	86.11 ± 0.34	52.33 ± 1.55	43.18 ± 2.10	36.63 ± 1.10	73.80 ± 0.59	43.29 ± 2.36	36.56 ± 3.28	32.17 ± 3.27
$\text{VIB}(\mathcal{L}_{GCE})$	85.70 ± 0.08	54.15 ± 1.85	44.84 ± 3.00	34.72 ± 2.43	78.88 ± 0.27	43.27 ± 1.56	31.24 ± 1.42	24.23 ± 1.45
SIB	89.99 ± 0.08	56.48 ± 2.50	46.62 ± 2.41	38.14 ± 2.37	70.58 ± 0.50	43.39 ± 2.83	33.40 ± 2.87	27.89 ± 2.93
(ELR+)+VIB	92.65 ± 0.27	$\underline{39.88 \pm 0.74}$	23.16 ± 0.40	14.60 ± 0.39	86.68 ± 0.25	42.72 ± 0.24	26.44 ± 0.64	14.70 ± 0.70
Promix+VIB	92.35 ± 0.38	51.27 ± 1.53	36.43 ± 0.65	20.49 ± 1.79	91.24 ± 0.28	52.88 ± 1.46	36.05 ± 0.68	23.79 ± 0.14
LaT-IB	94.17 ± 0.12	69.38 ± 1.23	60.66 ± 2.03	49.64 ± 2.27	87.95 ± 0.22	64.36 ± 1.67	54.18 ± 2.53	43.91 ± 3.05

Table 4: Classification accuracy (%) on CIFAR-10N (aggre and worst) under different adversarial perturbation levels. For Denoise + IB methods, adversarial attacks are applied in both stages: the VIB model is trained using the output of a denoising model that has itself been attacked. All the best results are highlighted in **bold**, and the second-best results are underlined.

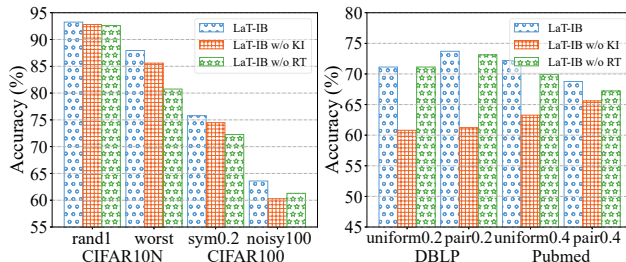


Figure 3: Ablation study.

role of each phase in enhancing model robustness, we design two ablated variants:

- **LaT-IB (w/o KI):** We remove the Knowledge Injection period, thus $\max(I(Y_n; S), I(Y_c; T)) \leq K$ is not satisfied, weakening the ability to map $S \rightarrow Y_c$ and $T \rightarrow Y_n$.
- **LaT-IB (w/o RT):** We remove the Robust Training period, meaning no further enhancement is applied to the representations from S, T . The LaT-IB model can only gain partial information from the three subsets.

Note that we do not design an ablation variant without the Warmup period, as it is essential for establishing basic classification capability and stable later training.

Results. Overall, the full LaT-IB method achieves the best performance under all noisy label settings as shown in Figure 3, demonstrating the importance of different periods in the framework. For image classification tasks (with larger samples), the Robust Training stage is particularly critical, while for graph-based tasks (with fewer samples), the Knowledge Injection stage proves more influential. These findings highlight the necessity of each training stage in achieving robust representations under noisy supervision.

5.5 Hyperparameter Sensitivity Analysis

We analyze the sensitivity of the model to the hyperparameter β , γ and δ . The coefficient β controls the feature compression term $I(\mathcal{D}; S, T)$, which encourages the model to learn noise invariant features. The coefficient γ controls the feature separation term $I(S; T|Y)$, which encourages the encoder $_{S,T}$ to capture clean and noisy representations respectively. δ regulates how much information the encoder $_{S,T}$ learns during the Knowledge Injection phase.

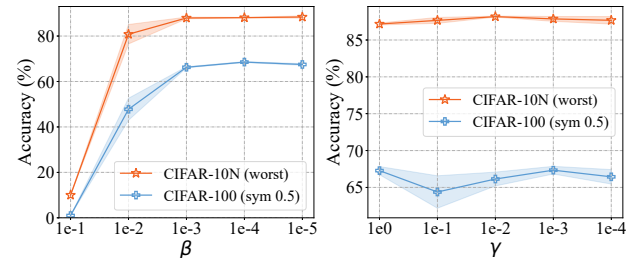


Figure 4: The influence of β and γ .

Results. We observe that a large β can dominate training and cause collapse as shown in Figure 4, indicating that $I(\mathcal{D}; S, T)$ partially limits the model’s expressiveness. However, our method is more tolerant to β than the original VIB, which fails to train on CIFAR-10 with 50% symmetric noise at $\beta = 0.01$. In contrast, our model performs better as β decreases because the input compression level is reduced.

We also observe that the model’s sensitivity to γ varies across noisy settings, highlighting the importance of the separation term $I(S; T|Y)$ under different types of noise.

For δ , a too-small δ limits the encoder’s training data exposure, while a too-large δ causes the encoders to converge, reducing their ability to separate clean and noisy information. More detailed results in Appendix E.6.

6 Conclusion

In this work, we propose **LaT-IB**, a novel yet principled IB framework that enables robust representation learning under label noise while preserving the principle of learning minimally sufficient representations. We disentangle features into representations related to clean and noisy label spaces, and theoretically demonstrate the noise-separating effect of our method through upper and lower bounds analysis. Furthermore, we design a three-phase training framework comprising Warmup, Knowledge Injection and Robust Training, that facilitates the extraction of “Minimal-Sufficient-Clean” representations. Extensive experiments across diverse noisy environments validate the superior performance of LaT-IB compared to existing IB-based methods, highlighting its potential to efficiently advance the practical application of IB theory in real-world learning scenarios with label noise.

Acknowledgments

The corresponding author is Qingyun Sun. This work is supported by NSFC under grants No.62427808 and No.62225202, and by the Fundamental Research Funds for the Central Universities. We extend our sincere thanks to all reviewers for their valuable efforts.

References

- Alemi, A. A.; Fischer, I.; Dillon, J. V.; and Murphy, K. 2017. Deep Variational Information Bottleneck. In *International Conference on Learning Representations*.
- Arpit, D.; Jastrzebski, S.; Ballas, N.; Krueger, D.; Bengio, E.; Kanwal, M. S.; Maharaj, T.; Fischer, A.; Courville, A.; Bengio, Y.; et al. 2017. A closer look at memorization in deep networks. In *International conference on machine learning*, 233–242. PMLR.
- Fano, R. 1952. Class notes for course 6.574: Transmission of information. *Lecture Notes*.
- Fu, X.; Wang, J.; Gao, Y.; Sun, Q.; Yuan, H.; Li, J.; and Li, X. 2025. Discrete curvature graph information bottleneck. In *Proceedings of the AAAI Conference on Artificial Intelligence*, volume 39, 16666–16673.
- Goodfellow, I. J.; Shlens, J.; and Szegedy, C. 2015. Explaining and Harnessing Adversarial Examples. In Bengio, Y.; and LeCun, Y., eds., *3rd International Conference on Learning Representations, ICLR 2015, San Diego, CA, USA, May 7-9, 2015, Conference Track Proceedings*.
- Harris, E.; Marcu, A.; Painter, M.; Niranjan, M.; Prügel-Bennett, A.; and Hare, J. 2020. Fmix: Enhancing mixed sample data augmentation. *arXiv preprint arXiv:2002.12047*.
- Hu, S.; Lou, Z.; Yan, X.; and Ye, Y. 2024. A survey on information bottleneck. *IEEE Transactions on Pattern Analysis and Machine Intelligence*.
- Kolchinsky, A.; Tracey, B. D.; and Wolpert, D. H. 2019. Nonlinear information bottleneck. *Entropy*, 21(12): 1181.
- Krizhevsky, A.; Hinton, G.; et al. 2009. Learning multiple layers of features from tiny images.
- Li, B.; Xie, X.; Lei, H.; Fang, R.; and Kang, Z. 2025. Simplified PCNet with robustness. *Neural Networks*, 184: 107099.
- Liu, S.; Niles-Weed, J.; Razavian, N.; and Fernandez-Granda, C. 2020. Early-learning regularization prevents memorization of noisy labels. *Advances in neural information processing systems*, 33: 20331–20342.
- Menon, A. K.; Jayasumana, S.; Rawat, A. S.; Jain, H.; Veit, A.; and Kumar, S. 2020. Long-tail learning via logit adjustment. *arXiv preprint arXiv:2007.07314*.
- Pan, S.; Wu, J.; Zhu, X.; Zhang, C.; and Wang, Y. 2016. Tri-party deep network representation. In *International Joint Conference on Artificial Intelligence 2016*, 1895–1901. Association for the Advancement of Artificial Intelligence (AAAI).
- Pan, Z.; Niu, L.; Zhang, J.; and Zhang, L. 2021. Disentangled information bottleneck. In *Proceedings of the AAAI Conference on Artificial Intelligence*, volume 35, 9285–9293.
- Patel, D.; and Sastry, P. 2023. Adaptive sample selection for robust learning under label noise. In *Proceedings of the IEEE/CVF Winter Conference on Applications of Computer Vision*, 3932–3942.
- Pensia, A.; Jog, V.; and Loh, P.-L. 2020. Extracting robust and accurate features via a robust information bottleneck. *IEEE Journal on Selected Areas in Information Theory*, 1(1): 131–144.
- Sen, P.; Namata, G.; Bilgic, M.; Getoor, L.; Galligher, B.; and Eliassi-Rad, T. 2008. Collective classification in network data. *AI magazine*, 29(3): 93–93.
- Shamir, O.; Sabato, S.; and Tishby, N. 2010. Learning and generalization with the information bottleneck. *Theoretical Computer Science*, 411(29-30): 2696–2711.
- Song, H.; Kim, M.; and Lee, J.-G. 2019. Selfie: Refurbishing unclean samples for robust deep learning. In *International conference on machine learning*, 5907–5915. PMLR.
- Song, H.; Kim, M.; Park, D.; and Lee, J.-G. 2019. How does early stopping help generalization against label noise? *arXiv preprint arXiv:1911.08059*.
- Song, H.; Kim, M.; Park, D.; Shin, Y.; and Lee, J.-G. 2022. Learning from noisy labels with deep neural networks: A survey. *IEEE transactions on neural networks and learning systems*, 34(11): 8135–8153.
- Sugiyama, M.; Suzuki, T.; and Kanamori, T. 2012. Density-ratio matching under the bregman divergence: a unified framework of density-ratio estimation. *Annals of the Institute of Statistical Mathematics*, 64: 1009–1044.
- Tishby, N.; Pereira, F. C.; and Bialek, W. 2000. The information bottleneck method. *arXiv preprint physics/0004057*.
- Wang, Y.; Ma, X.; Chen, Z.; Luo, Y.; Yi, J.; and Bailey, J. 2019. Symmetric cross entropy for robust learning with noisy labels. In *Proceedings of the IEEE/CVF international conference on computer vision*, 322–330.
- Wang, Z.; Sun, D.; Zhou, S.; Wang, H.; Fan, J.; Huang, L.; and Bu, J. 2024. NoisyGL: A Comprehensive Benchmark for Graph Neural Networks under Label Noise. *arXiv preprint arXiv:2406.04299*.
- Wei, H.; Feng, L.; Chen, X.; and An, B. 2020. Combating noisy labels by agreement: A joint training method with co-regularization. In *Proceedings of the IEEE/CVF conference on computer vision and pattern recognition*, 13726–13735.
- Wei, J.; Zhu, Z.; Cheng, H.; Liu, T.; Niu, G.; and Liu, Y. 2022. Learning with Noisy Labels Revisited: A Study Using Real-World Human Annotations. In *International Conference on Learning Representations*.
- Wu, T.; Ren, H.; Li, P.; and Leskovec, J. 2020. Graph information bottleneck. *Advances in Neural Information Processing Systems*, 33: 20437–20448.
- Xiao, R.; Dong, Y.; Wang, H.; Feng, L.; Wu, R.; Chen, G.; and Zhao, J. 2023. ProMix: combating label noise via maximizing clean sample utility. In *Proceedings of the Thirty-Second International Joint Conference on Artificial Intelligence*, 4442–4450.

Xie, S.; Ma, S.; Ding, M.; Shi, Y.; Tang, M.; and Wu, Y. 2023. Robust information bottleneck for task-oriented communication with digital modulation. *IEEE Journal on Selected Areas in Communications*, 41(8): 2577–2591.

Yang, H.; Wu, Y.; Wen, D.; Zhou, Y.; and Shi, Y. 2025. Structured IB: Improving Information Bottleneck with Structured Feature Learning. In *Proceedings of the AAAI Conference on Artificial Intelligence*, volume 39, 21922–21928.

Yang, L.; Zheng, J.; Wang, H.; Liu, Z.; Huang, Z.; Hong, S.; Zhang, W.; and Cui, B. 2023. Individual and structural graph information bottlenecks for out-of-distribution generalization. *IEEE Transactions on Knowledge and Data Engineering*, 36(2): 682–693.

Yuan, H.; Sun, Q.; Fu, X.; Ji, C.; and Li, J. 2024. Dynamic graph information bottleneck. In *Proceedings of the ACM Web Conference 2024*, 469–480.

Yuan, J.; Luo, X.; Qin, Y.; Zhao, Y.; Ju, W.; and Zhang, M. 2023. Learning on graphs under label noise. In *ICASSP 2023-2023 IEEE International Conference on Acoustics, Speech and Signal Processing (ICASSP)*, 1–5. IEEE.

Zhang, H.; Cisse, M.; Dauphin, Y. N.; and Lopez-Paz, D. 2018. mixup: Beyond Empirical Risk Minimization. In *International Conference on Learning Representations*.

Zhang, Z.; and Sabuncu, M. 2018. Generalized cross entropy loss for training deep neural networks with noisy labels. *Advances in neural information processing systems*, 31.

Zhou, Z.; Yao, J.; Liu, J.; Guo, X.; Yao, Q.; He, L.; Wang, L.; Zheng, B.; and Han, B. 2023. Combating bilateral edge noise for robust link prediction. *Advances in Neural Information Processing Systems*, 36: 21368–21414.

Zhu, Y.; Feng, L.; Deng, Z.; Chen, Y.; Amor, R.; and Witbrock, M. 2024. Robust node classification on graph data with graph and label noise. In *Proceedings of the AAAI conference on artificial intelligence*, volume 38, 17220–17227.

A Code Source

The code for LaT-IB is publicly available at: <https://github.com/RingBDStack/LaT-IB>.

B Algorithms and Complexity Analysis

B.1 The Overall Process of LaT-IB

The overall training pipeline of LaT-IB is outlined in Algorithm B.1.

Algorithm B.1: The Overall Process of LaT-IB

Input: Input data \mathcal{D} with label Y , epoch number of each period $E_{\text{Warmup}}, E_{\text{Injection}}, E_{\text{Robust}}$, overall epoch number E

Output: Predicted label \hat{Y}

```

1: Parameter initialization
2: for epoch  $i = 1, \dots, E$  do
3:   Encode inputs to obtain  $(\mu_S, \sigma_S), (\mu_T, \sigma_T)$ 
4:   Decode the reparameterized embedding to generate
   predictions  $(\hat{y}_S, \hat{y}_T)$ 
5:   if  $i \leq E_{\text{Warmup}}$  then
6:     Optimize the encoderS with Eq. (13)
7:   end if
8:   if  $E_{\text{Warmup}} < i \leq E_{\text{Injection}}$  then
9:     Obtain Clean/Noise/Uncertain Set using InfoJS se-
     lector
10:    Optimize the LaT-IB model with Eq. (15) and (16)
11:  end if
12:  if  $i > E_{\text{Injection}}$  then
13:    Optimize the LaT-IB model with Eq. (18)
14:    Optimize the discriminator with Eq. (19)
15:  end if
16: end for

```

B.2 InfoJS Selector Algorithms Details

Algorithm B.2 implements a sample selection scheme based on MI and JS divergence.

B.3 $\mathcal{L}_{\text{ConCE}}$ Algorithms Details

Proposition 4.1 states:

$$-I(Y; S, T) \leq -\max(I(Y; S), I(Y; T)). \quad (\text{B.1})$$

Further reformulated as a cross-entropy loss, this provides an implementation method for $I(Y; S, T)$:

$$-I(Y; S, T) \leq \sum_i \min(\mathcal{L}(\hat{y}_{S,i}, y_i), \mathcal{L}(\hat{y}_{T,i}, y_i)). \quad (\text{B.2})$$

In the loss function design, we tailor the loss for two scenarios: image classification (many samples) and node classification (few samples).

Graph Tasks. First, we present the loss function design for the node classification task under the few-sample condition, as it is closest to Equation (B.2). Since the min function is not continuous and may hinder model learning, we instead use the smooth approximation:

$$f(a, b) = \frac{1}{\beta} \cdot \log(\exp(-\beta \cdot a) + \exp(-\beta \cdot b)). \quad (\text{B.3})$$

Algorithm B.2: InfoJS Selector

Input: Trained model f_θ , data (\mathcal{D}, Y) , selection ratio δ

Output: Binary selection mask: $\text{mask}_S, \text{mask}_T$

```

1: Run  $f_\theta$  to obtain  $(\mu_S, \sigma_S), (\mu_T, \sigma_T)$  and predictions
    $(\hat{y}_S, \hat{y}_T)$ 
2: Compute  $I(S; Y)$ :  $\ell_S \leftarrow \mathcal{L}_{\text{CE}}(\hat{y}_S, y)$  {Eq. (10)}
3: Compute JS divergence:  $JS \leftarrow D_{\text{JS}}(\mu_S, \sigma_S, \mu_T, \sigma_T)$ 
4: Initialize  $\text{mask}_S, \text{mask}_T$ 
5: for each class  $j = 1, \dots, C$  do
6:    $\mathcal{I}_j \leftarrow$  indices of class- $j$  samples in  $\mathcal{M}$ 
7:    $k_j \leftarrow \max(1, \min(\lceil \delta \cdot |\mathcal{I}_j| \rceil, |\mathcal{D}|/C))$ 
8:   Select top- $k_j$  and bottom- $k_j$  samples by  $\ell_S$  and up-
     date  $\text{mask}_S, \text{mask}_T$ 
9:   Select top- $k_j$  and bottom- $k_j$  samples by  $JS$  and up-
     date  $\text{mask}_S, \text{mask}_T$ 
10: end for
11: return  $\text{mask}_S, \text{mask}_T$  { $\text{mask}_S$  for clean set;  $\text{mask}_T$  for
    noise set}

```

Notably, as $b \rightarrow +\infty$, this expression becomes equivalent to $\min(a, b)$.

Algorithm B.3: $\mathcal{L}_{\text{ConCE}}$ for node classification

Input: Predictions $prob_1, prob_2$; Labels y ; Threshold β

Output: Final loss value $\mathcal{L}_{\text{ConCE}}$

```

1:  $a \leftarrow \mathcal{L}_{\text{CE}}(prob_1, y)$  {Per-sample  $\mathcal{L}_{\text{CE}}$ }
2:  $b \leftarrow \mathcal{L}_{\text{CE}}(prob_2, y)$ 
3:  $L \leftarrow \frac{1}{\beta} \cdot \log(\exp(-\beta \cdot a) + \exp(-\beta \cdot b))$  {Eq. (B.3)}
4: return Mean( $L$ )

```

Image Tasks. We then directly apply Algorithm B.3 to the image classification task and observe that it causes lazy training, where the model tends to produce identical outputs. We hypothesize that this behavior arises because: as the number of training samples increases, the gradient contributions from noisy samples become diluted. Meanwhile, Algorithm B.3 imposes a strict separation, causing each encoder to receive only a limited portion of the input data. As a result, when the predictions from the two encoders become overly similar, the model lacks sufficient supervision signals, potentially leading to training collapse.

To address this issue, we train both encoders on the samples where the two prediction heads produce consistent outputs, rather than assigning them to a single encoder. This significantly increases the amount of usable information for each encoder. Moreover, we relax the condition in Equation B.2 to:

$$\begin{aligned} -I(Y; S, T) &\leq \sum_i \min(\mathcal{L}(\hat{y}_{S,i}, y_i), \mathcal{L}(\hat{y}_{T,i}, y_i)) \\ &\leq \sum_i \max(\mathcal{L}(\hat{y}_{S,i}, y_i), \mathcal{L}(\hat{y}_{T,i}, y_i)) \end{aligned} \quad (\text{B.4})$$

The final loss function is shown in Algorithm B.4.

Algorithm B.4: \mathcal{L}_{ConCE} for image classification

Input: Predictions $prob_1, prob_2$; Labels y ; Threshold t
Output: Final loss value \mathcal{L}_{ConCE}

- 1: Compute $a \leftarrow \mathcal{L}_{CE}(prob_1.\text{copy}(), y)$
- 2: Compute $b \leftarrow \mathcal{L}_{CE}(prob_2.\text{copy}(), y)$
- 3: $pred_1 \leftarrow \arg \max(prob_1.\text{copy}())$ {Per-sample \mathcal{L}_{CE} }
- 4: $pred_2 \leftarrow \arg \max(prob_2.\text{copy}())$
- 5: $mask_a \leftarrow (a < b)$
- 6: $mask_b \leftarrow (a > b) \vee (pred_1 = pred_2)$ {The second part prevents T from learning nothing.}
- 7: **if** $\sum(pred_1 = pred_2)/|y| > t$ **then**
- 8: $mask_a \leftarrow (a < b) \vee (pred_1 = pred_2)$
- 9: $mask_b \leftarrow (a > b)$
- 10: **end if**
- 11: Initialize $y_1 \leftarrow y, y_2 \leftarrow y$
- 12: Replace $y_1[mask_a] \leftarrow pred_1[mask_a]$ {Focus on clean samples}
- 13: Replace $y_2[mask_b] \leftarrow pred_2[mask_b]$ {Focus on noise samples}
- 14: $loss_1 \leftarrow \mathcal{L}_{CE}(prob_1, y_1)$
- 15: $loss_2 \leftarrow \mathcal{L}_{CE}(prob_2, y_2)$
- 16: **return** $(loss_1 + loss_2)/2$

B.4 Time Consumption

We adopt the constant definitions from Section 3. For Algorithm B.2, the \mathcal{L}_{CE} has a time complexity of $\mathcal{O}(NC)$. The JS divergence, computed between all sample pairs, requires $\mathcal{O}(N^2k)$ operations, where k is the dimensionality of the Gaussian embeddings. Assuming class-balanced data, the per-class selection of top- k and bottom- k samples involves sorting subsets of size approximately N/C , giving a total sorting complexity of $\mathcal{O}(N \log(N/C))$. Overall, the dominant term is $\mathcal{O}(N^2k)$, since typically $C \ll N$, making the pairwise divergence computation the main computational bottleneck.

Algorithms B.3 and B.4 perform a finite number of cross-entropy loss computations. Therefore, their overall time complexity is equivalent to that of the cross-entropy loss, which is $\mathcal{O}(NC)$.

To further assess the efficiency of different methods, we report the training time consumption of several top-performing approaches.

Image Classification. We selected three baselines including VIB, (ELR+)+VIB and (Promix²)+VIB as well as compared their time consumption under the condition of achieving a performance like Table 2 on CIFAR-10N dataset, as shown in the Table B.1. The results demonstrate that although our model incurs higher computation than VIB, it achieves better performance within fewer epochs, and overall outperforms two-stage models in terms of efficiency.

²For the Promix method, strictly following the original experimental setup results in a runtime exceeding 24 hours, leading to out-of-time (OOT) termination. To address this, we reduced the number of training epochs, with only a minor performance drop, to ensure timely completion.

Method	VIB	(ELR+)+VIB	(Promix)+VIB	LaT-IB
Time (h)	1.6	4.9+1.6	12.9+1.6	5.18
Epoch	100	200+100	300+100	200
Per Epoch (min)	0.94	1.30	2.18	1.55

Table B.1: Comparison of training time consumption (IC)

Node Classification. We selected GIB, GIB (\mathcal{L}_{GCE}) and RNCGLN+GIB as baselines. Table B.2 presents the results on the DBLP dataset, supporting similar conclusions as in the image classification task. Notably, although RNCGLN achieves strong performance, it incurs significant time overhead, as also reported in NoisyGL (Wang et al. 2024).

Method	GIB	GIB (\mathcal{L}_{GCE})	RNCGLN+GIB	LaT-IB
Time (s)	37.8	37.8	3445.4+37.8	55.9
Epoch	100	100	500+100	100
Per Epoch (s)	0.38	0.38	5.80	0.56

Table B.2: Comparison of training time consumption (NC)

We evaluate the time cost at each period of the pipeline. The results are shown in Figure B.1. The results indicate that for image tasks with a **large** number of samples, Knowledge Injection consumes the most time, which aligns with our theoretical time complexity analysis. In contrast, for graph tasks with **fewer** samples, the time cost of Knowledge Injection is slightly lower than that of Robust Training. We speculate that this is due to lower actual time complexity than the theoretical value, possibly resulting from low-level computational optimizations, and the relatively small sample size helps offset part of the time overhead.

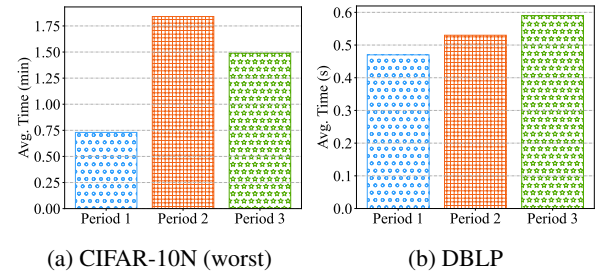


Figure B.1: Time Consumption Analysis

C Proofs

In this section, we present the relevant proofs from the paper. We first restate the statements to be proved, followed by detailed proofs.

C.1 The proof of Theorem 1.1

Theorem C.1 (Cumulative Degradation). *In the two-stage approach, f_1 is used to modify the labels $Y' = f_1(\mathcal{D})$, and f_2 is responsible for extracting valid information from \mathcal{D} while approximating the prediction result to $f_1(\mathcal{D})$. For one-stage model $g(\mathcal{D})$, it extracts the relevant information*

while removing noise. If the denoising abilities of f_1 and g are the same, the following inequality holds:

$$P(f_2(\mathcal{D}) \neq g(\mathcal{D})) \geq \frac{H(Y'|\mathcal{D}) - 1}{\log(|\mathcal{Y}| - 1)}, \quad (\text{C.1})$$

where \mathcal{Y} denotes the support of Y , and $|\mathcal{Y}|$ denotes the number of elements in \mathcal{Y} . The two models perform identically iff f_2 achieves the error lower bound and $H(Y'|\mathcal{D}) = 0$.

Proof. Without loss of generality, we illustrate this using the image classification task, where $\mathcal{D} = X$.

We begin by introducing **Fano's inequality** (Fano 1952): Let the discrete random variables X and Y denote the input and output messages, respectively, with joint distribution $P(x, y)$. Let e represent the event of an error, i.e., $X \neq \hat{X}$, where $\hat{X} = f(Y)$ is an estimate of X . Then **Fano's inequality** states:

$$H(X|Y) \leq H_b(e) + P(e) \log(|\mathcal{X}| - 1), \quad (\text{C.2})$$

where \mathcal{X} denotes the support set of the random variable X , and $|\mathcal{X}|$ is its cardinality (i.e., the number of elements in \mathcal{X}). Here, $H(X|Y) = -\sum_{i,j} P(x_i, y_j) \log P(x_i|y_j)$ is the conditional entropy, $P(e) = P(X \neq \hat{X})$ is the probability of a communication error, and $H_b(e) = -P(e) \log P(e) - (1 - P(e)) \log(1 - P(e))$ is the binary entropy.

Part 1: Consider the second stage f_2 of the two-stage model, whose input Y' serves as a reference for the final model output $f_2(x)$. According to the inequality above, we have:

$$H(Y'|X) \leq H_b(e) + P(e) \log(|\mathcal{Y}| - 1), \quad (\text{C.3})$$

where $P(e) := P(f_2(x) \neq f_1(x))$. Since the binary entropy has an upper bound of 1, the lower bound of the error probability is:

$$\begin{aligned} H(Y'|X) &\leq H_b(e) + P(e) \log(|\mathcal{Y}| - 1) \\ &\leq 1 + P(e) \log(|\mathcal{Y}| - 1), \end{aligned} \quad (\text{C.4})$$

Given the assumption that f_1 and g have the same denoising capability, we can, without loss of generality, assume $f_1(x) = g(x)$, thus:

$$P(f_2(x) \neq g(x)) = P(e) \geq \frac{H(Y'|X) - 1}{\log(|\mathcal{Y}| - 1)}. \quad (\text{C.5})$$

Part 2: When the two models behave identically, i.e., $P(f_2(x) \neq g(x)) = 0$, from inequality C.3 we know that $H(Y'|X) \leq 0$. Since entropy is non-negative, it follows that $H(Y'|X) = 0$. At this point, f_2 has optimized its classification error to the theoretical lower bound.

When $H(Y'|X) = 0$, it is easy to see that $P(f_2(x) \neq g(x)) = 0$ satisfies inequality C.3. Since $P(f_2(x) \neq g(x)) \geq 0$, and 0 is the lower bound of the error rate, if f_2 reaches this bound, the performance of the two models is exactly the same. \square

C.2 The proof of Lemma 4.1 and 4.2

Lemma C.1 (Nuisance Invariance). *Taking the part of \mathcal{D} that does not contribute to Y as \mathcal{D}_n (\mathcal{D}_n is independent of Y), and considering the Markov chain $(Y, \mathcal{D}_n) \rightarrow \mathcal{D} \rightarrow (S, T)$, the following inequality holds:*

$$I(\mathcal{D}_n; S, T) \leq -I(Y; S, T) + I(\mathcal{D}; S, T). \quad (\text{C.6})$$

Proof. We proof this lemma in three steps.

Step 1: According to the property of the Markov chain, we have:

$$I(S, T; \mathcal{D}_n, Y|\mathcal{D}) = 0. \quad (\text{C.7})$$

And because:

$$\begin{aligned} &I(S, T; \mathcal{D}_n, Y|\mathcal{D}) \\ &= \underbrace{I(S, T; \mathcal{D}_n|\mathcal{D})}_{\geq 0} + \underbrace{I(S, T; Y|\mathcal{D}_n, \mathcal{D})}_{\geq 0} \\ &= 0. \end{aligned} \quad (\text{C.8})$$

So we have:

$$I(S, T; \mathcal{D}_n|\mathcal{D}) = I(S, T; Y|\mathcal{D}_n, \mathcal{D}) = 0 \quad (\text{C.9})$$

By expanding $I(S, T; \mathcal{D}, \mathcal{D}_n)$, we obtain:

$$\begin{aligned} I(S, T; \mathcal{D}, \mathcal{D}_n) &= I(S, T; \mathcal{D}) + I(S, T; \mathcal{D}_n|\mathcal{D}) \\ &= I(S, T; \mathcal{D}). \end{aligned} \quad (\text{C.10})$$

By an alternative expansion, we obtain:

$$I(S, T; \mathcal{D}, \mathcal{D}_n) = I(S, T; \mathcal{D}_n) + I(S, T; \mathcal{D}|\mathcal{D}_n). \quad (\text{C.11})$$

Combining Eq. (C.10) and (C.11), we obtain the following equality:

$$I(S, T; \mathcal{D}) = I(S, T; \mathcal{D}_n) + I(S, T; \mathcal{D}|\mathcal{D}_n). \quad (\text{C.12})$$

Step 2: By expanding $I(S, T; Y, \mathcal{D}|\mathcal{D}_n)$, we obtain:

$$I(S, T; Y, \mathcal{D}|\mathcal{D}_n) = I(S, T; \mathcal{D}|\mathcal{D}_n) + I(S, T; Y|\mathcal{D}, \mathcal{D}_n). \quad (\text{C.13})$$

Since we have $I(S, T; Y|\mathcal{D}, \mathcal{D}_n) = 0$:

$$I(S, T; Y, \mathcal{D}|\mathcal{D}_n) = I(S, T; \mathcal{D}|\mathcal{D}_n). \quad (\text{C.14})$$

Similarly, by expanding in another way:

$$I(S, T; Y, \mathcal{D}|\mathcal{D}_n) = I(S, T; Y|\mathcal{D}_n) + I(S, T; \mathcal{D}|Y, \mathcal{D}_n). \quad (\text{C.15})$$

Combining Eq. (C.14) and (C.15), we obtain

$$\begin{aligned} I(S, T; \mathcal{D}|\mathcal{D}_n) &= I(S, T; Y|\mathcal{D}_n) + I(S, T; \mathcal{D}|Y, \mathcal{D}_n) \\ &\Rightarrow I(S, T; \mathcal{D}|\mathcal{D}_n) \geq I(S, T; Y|\mathcal{D}_n). \end{aligned} \quad (\text{C.16})$$

Step 3: Substituting Eq. (C.16) into Eq. (C.12), we obtain:

$$\begin{aligned} I(S, T; \mathcal{D}) &\geq I(S, T; \mathcal{D}_n) + I(S, T; Y|\mathcal{D}_n) \\ &= I(S, T; \mathcal{D}_n) + I(S, T; Y). \end{aligned} \quad (\text{C.17})$$

Therefore, we obtain the conclusion:

$$I(\mathcal{D}_n; S, T) \leq -I(Y; S, T) + I(\mathcal{D}; S, T). \quad (\text{C.18})$$

\square

Lemma C.2 (Feature Convergence). *Assuming that Y can potentially contain all information about Y_r and Y_n , the following inequality holds when $\max(I(Y_n; S), I(Y_r; T)) \leq \max(I(S; T), \varepsilon)/2 = K, \varepsilon \in \mathbb{R}$ is satisfied:*

$$-I(Y_r; S) - I(Y_n; T) - \varepsilon \leq -I(Y; S, T) + I(S; T|Y). \quad (\text{C.19})$$

Proof. By expanding the mutual information and combining the assumptions, we have:

$$\begin{aligned} & I(Y; S, T) \\ &= I(Y; S) + I(Y; T) - I(Y; S, T) \\ &= I(Y; S) + I(Y; T) - (I(S; T) - I(S; T|Y)) \\ &= I(Y; S) + I(Y; T) - I(S; T) + I(S; T|Y) \\ &= I(Y_r, Y_n; S) + I(Y_r, Y_n; T) - I(S; T) + I(S; T|Y) \\ &\leq I(Y_r; S) + I(Y_n; S) + I(Y_r; T) + I(Y_n; T) \\ &\quad - I(S; T) + I(S; T|Y). \end{aligned} \quad (\text{C.20})$$

Rearranging the terms, we obtain:

$$\begin{aligned} & -I(Y; S, T) + I(S; T|Y) \\ &\geq -I(Y_r; S) - I(Y_n; T) + (I(S; T) - I(Y_n; S) - I(Y_r; T)). \end{aligned} \quad (\text{C.21})$$

Now, we consider two cases:

Case 1: When $I(S, T) \geq \varepsilon$:

$$\begin{aligned} & -I(Y; S, T) + I(S; T|Y) \\ &\geq -I(Y_r; S) - I(Y_n; T) + (I(S; T) - I(Y_n; S) - I(Y_r; T)) \\ &\geq -I(Y_r; S) - I(Y_n; T). \end{aligned} \quad (\text{C.22})$$

Case 2: When $I(S, T) < \varepsilon$:

$$\begin{aligned} & -I(Y; S, T) + I(S; T|Y) \\ &\geq -I(Y_r; S) - I(Y_n; T) + (I(S; T) - I(Y_n; S) - I(Y_r; T)) \\ &\geq -I(Y_r; S) - I(Y_n; T) - I(Y_n; S) - I(Y_r; T) \\ &\geq -I(Y_r; S) - I(Y_n; T) - \varepsilon. \end{aligned} \quad (\text{C.23})$$

Thus, the conclusion is proven. \square

C.3 The proof of Proposition 4.1 ~ 4.4

Proposition C.1 (The upper bound of $-I(Y; S, T)$). *Given the label Y and the variable S, T that learns the characteristics of the real label space and the noise label space respectively, we have:*

$$-I(Y; S, T) \leq -\max(I(Y; S), I(Y; T)). \quad (\text{C.24})$$

Proof. Expand directly using the definition of mutual information:

$$\begin{aligned} I(Y; S, T) &= I(Y; S) + I(Y; T|S) \\ &= I(Y; T) + I(Y; S|T) \\ &\geq \max(I(Y; S), I(Y; T)) \end{aligned} \quad (\text{C.25})$$

So that $-I(Y; S, T) \leq -\max(I(Y; S), I(Y; T))$. \square

Proposition C.2 (The upper bound of $I(\mathcal{D}; S, T)$). *Let \mathcal{D}, S, T be random variables. Assume the probabilistic mapping $p(\mathcal{D}, S, T)$ follows the Markov chain $S \leftrightarrow \mathcal{D} \leftrightarrow T$. Then:*

$$I(\mathcal{D}; S, T) \leq I(\mathcal{D}; S) + I(\mathcal{D}; T). \quad (\text{C.26})$$

Proof. Without loss of generality, here we take $\mathcal{D} = X$ as an example to prove it.

Expanded by definition and processed over the probability distributions, we can obtain:

$$\begin{aligned} & I(\mathcal{D}; S, T) \\ &= \mathbb{E}_{p(x, s, t)} \log \frac{p(s, t, x)}{p(x)p(s, t)} \\ &= \mathbb{E}_{p(x, s, t)} \log \frac{p(x)p(s|x)p(t|x)}{p(x)p(s, t)} \\ &= \mathbb{E}_{p(x, s, t)} \log \left[\frac{p(s|x)p(x)}{p(x)p(s)} \cdot \frac{p(t|x)p(x)}{p(x)p(t)} \cdot \frac{p(s)p(t)}{p(s, t)} \right] \\ &= I(\mathcal{D}; S) + I(\mathcal{D}; T) - I(S; T) \\ &\leq I(\mathcal{D}; S) + I(\mathcal{D}; T) \end{aligned} \quad (\text{C.27})$$

\square

Proposition C.3 (Reformulation of $I(S, T|Y)$). *Given the label Y and the variable S, T , minimizing $I(S; T|Y)$ is equivalent to minimize $I(S, Y; T, Y)$.*

Proof.

$$\begin{aligned} & I(S; T|Y) \\ &= \int_y p(y) \iint_{s,t} p(s, t|y) \log \frac{p(s, t|y)}{p(s|y)p(t|y)} ds dt dy \\ &= \iiint_{(s,t,y)} p(s, t, y) \log \frac{p(s, t, y)}{p(s, y)p(t, y)} p(y) ds dt dy \\ &= \mathbb{E}_{p(s,t,y)} \log \frac{p(s, t, y)}{p(s, y)p(t, y)} + \mathbb{E}_{p(y)} \log p(y) \\ &= I(S, Y; T, Y) - H(Y) \end{aligned} \quad (\text{C.28})$$

Since $H(Y)$ is a constant, it follows that $I(S; T|Y) \propto I(S, Y; T, Y)$, thus proved. \square

Proposition C.4 (Reformulation of the condition in Eq. (8): $\max(I(Y_n; S), I(Y_c; T)) \leq K$). *Minimizing $I(Y_r; T)$ and $I(Y_n; S)$ is equivalent to increase $I(Y_n; T)$ and $I(Y_r; S)$.*

Proof. For S , with limited capacity ($I(Y; S) \leq A$), we have:

$$I(Y_r; S) + I(Y_n; S) \leq I(Y; S) + I(Y_r; Y_n) \leq A + \text{const} \quad (\text{C.29})$$

Similarly, for T , enlarging one part constrains the other under limited capacity. \square

C.4 The proof of Eq. (10): $\max I(Y; Z)$ is equivalent to $\min \mathcal{L}_{CE}$

Proof.

$$\begin{aligned} I(Y; Z) &= \iint_{(y,z)} p(y, z) \log \frac{p(y, z)}{p(y)p(z)} dy dz \\ &= \iint_{(y,z)} p(y, z) \log \frac{p(y|z)}{p(y)} dy dz \\ &= \mathbb{E}_{p(y,z)} (\log(q_\theta(y|z))) + \\ &\quad \mathbb{E}_{p(z)} (D_{KL}(p(y|z) \| q_\theta(y|z))) + H(Y) \\ &\geq \mathbb{E}_{p(y,z)} (\log(q_\theta(y|z))) = -\mathcal{L}_{CE}(Z, Y), \end{aligned} \quad (\text{C.30})$$

where $q_{\theta_i}(\cdot)$ is variational approximation of $p(\cdot)$. \square

D Implement Details

D.1 Implement Details of $\mathcal{L}_{Minimal}$

As established in Proposition 4.2, minimizing the $I(\mathcal{D}; S, T)$ objective reduces to minimizing $I(\mathcal{D}; Z)$, where $Z \in \{S, T\}$. We now discuss the methodology for estimating and optimizing $I(\mathcal{D}; Z)$.

The input is an image. In this case, $\mathcal{D} = X$, i.e., the input to the model consists solely of image features. Therefore, minimizing $I(\mathcal{D}; Z)$ reduces to minimizing the divergence between the approximate posterior and a fixed prior.

Proof. Expanded via the definition of mutual information:

$$\begin{aligned} I(X; Z) &= \iint_{(x,z)} p(x, z) \log \frac{p(x, z)}{p(x)p(z)} dx dz \\ &= \int_x p(x) \left[\int_z p(z|x) \log \frac{p(z|x)}{q(z)} dz \right] dx - \int_z p(z) \log \frac{p(z)}{q(z)} dz \\ &= \int_x p(x) [D_{KL}[p(z|x) \| q(z)]] dx - D_{KL}[p(z) \| q(z)] \\ &\leq \mathbb{E}_{p(x)} [D_{KL}[p(z|x) \| q(z)]]. \end{aligned} \quad (\text{D.1}) \quad \square$$

Since $q(z)$ represents the marginal distribution of the latent variable and is not constrained during training, we can assume without loss of generality that $q(z) \sim \mathcal{N}(0, I_n)$. The encoder maps input features to a Gaussian distribution, i.e., $p(z|x) \sim \mathcal{N}(\mu_n, \sigma_n)$. In this case, the KL divergence between two Gaussian distributions admits a closed-form solution and can be computed as:

$$D_{KL}[p(z|x) \| q(z)] = \frac{1}{2} \sum_{i=1}^n (\mu_i^2 + \sigma_i^2 - \log \sigma_i^2 - 1). \quad (\text{D.2})$$

The input is a graph. In this case, the input data is the graph $\mathcal{D} = \mathcal{G} = (X, A)$, where X denotes node features and A denotes the adjacency matrix. As a result, the estimation of the mutual information $I(\mathcal{D}; Z)$ becomes more intricate compared to scenarios with only feature inputs.

Following the framework of Graph Information Bottleneck (GIB), we consider two groups of indices $S_X, S_A \subseteq [L]$ that satisfy the Markovian dependence. Specifically, we assume $\mathcal{D} \perp Z_X^{(L)} \setminus \{Z_X^{(l)}\}_{l \in S_X} \cup \{Z_A^{(l)}\}_{l \in S_A}$, where $Z_X^{(l)}$ denotes the node feature representation at layer l , and $Z_A^{(l)}$ denotes the structural representation at layer l . Based on this condition, for any set of distributions $\mathbb{Q}(Z_X^{(l)})$ with $l \in S_X$, and $\mathbb{Q}(Z_A^{(l)})$ with $l \in S_A$, the following upper bound holds:

$$I(\mathcal{D}; Z_X^{(L)}) \leq \sum_{l \in S_A} \text{AIB}^{(l)} + \sum_{l \in S_X} \text{XIB}^{(l)}, \quad (\text{D.3})$$

where $\text{AIB}^{(l)}$ and $\text{XIB}^{(l)}$ denote the information contributions from the adjacency and feature paths, respectively, and are defined as:

$$\begin{aligned} \text{AIB}^{(l)} &= \mathbb{E} \left[\log \frac{\mathbb{P}(Z_A^{(l)} | A, Z_X^{(l-1)})}{\mathbb{Q}(Z_A^{(l)})} \right], \\ \text{XIB}^{(l)} &= \mathbb{E} \left[\log \frac{\mathbb{P}(Z_X^{(l)} | Z_X^{(l-1)}, Z_A^{(l)})}{\mathbb{Q}(Z_X^{(l)})} \right]. \end{aligned} \quad (\text{D.4})$$

For the structural branch, we adopt a Bernoulli-based KL divergence estimator:

$$\widehat{\text{AIB}}^{(l)} = \sum_{v \in V, t \in [\mathcal{T}]} D_{KL} \left(\text{Bernoulli}(\phi_{v,t}^{(l)}) || \text{Bernoulli}(\alpha) \right), \quad (\text{D.5})$$

where $\phi^{(l)}_{v,t}$ denotes the probability of an edge between node v and its t -hop neighbors, and α is the prior class probability.

To estimate $\text{XIB}^{(l)}$, we model $\mathbb{Q}(Z_X^{(l)})$ as a mixture of Gaussians with learnable parameters. For any node v , we assume $Z_{X,v}^{(l)} \sim \sum_{i=1}^m w_i \mathcal{N}(\mu_{0,i}, \sigma_{0,i}^2)$, where $w_i, \mu_{0,i}$ and $\sigma_{0,i}$ are shared parameters across all nodes, and $Z_{X,v} \perp Z_{X,u}$ if $v \neq u$. We compute:

$$\begin{aligned} \widehat{\text{XIB}}^{(l)} &= \log \frac{\mathbb{P}(Z_X^{(l)} | Z_X^{(l-1)}, Z_A^{(l)})}{\mathbb{Q}(Z_X^{(l)})} \\ &= \sum_{v \in V} \log \Phi(Z_{X,v}^{(l)}; \mu_v, \sigma_v^2) \\ &\quad - \log \left(\sum_{i=1}^m w_i \Phi(Z_{X,v}^{(l)}; \mu_i, \sigma_{0,i}^2) \right), \end{aligned} \quad (\text{D.6})$$

where $\Phi(\cdot)$ denotes the probability density function of a Gaussian distribution.

In conclusion, we select proper sets of indices S_X, S_A and use substitution:

$$I(\mathcal{D}, Z) \leftarrow \sum_{l \in S_A} \widehat{\text{AIB}}^{(l)} + \sum_{l \in S_X} \widehat{\text{XIB}}^{(l)}. \quad (\text{D.7})$$

More detailed content and proof can be found in GIB (Wu et al. 2020).

D.2 Implement Details of Knowledge Injection

Building on the proven success of mixup-based techniques in computer vision, we apply FMix (Harris et al. 2020) for image data augmentation across both clean and noisy subsets. To counteract potential class bias during training, we incorporate Debiased Margin-based Loss (Xiao et al. 2023) and Debiased Pseudo Labeling (Menon et al. 2020), fostering unbiased model predictions.

D.3 Implement Details of Robust Training

To further improve model performance, we perform certain modifications to the label Y during robust training period.

For image classification, every k epochs, the model predictions are combined with the original labels using exponential moving average to replace the original labels.

For node classification, at each epoch, the labels of samples with prediction confidence higher than a threshold τ are replaced with the model’s predicted results.

E Experiments Details and Results

E.1 Data

Image Classification. We select CIFAR-based datasets to simulate both synthetic and real-world label noise. To mitigate the risk of overfitting to a specific dataset, we also include the Animal-10N dataset. Specifically:

- **CIFAR-10/100 (Krizhevsky, Hinton et al. 2009)³:** These are classic image classification datasets with 10 and 100 categories, respectively. By constructing a noise transition matrix, we introduce symmetric noise (Sym Noise, where each noisy label is uniformly sampled from all classes) and asymmetric noise (Asym Noise, where each class is flipped to a specific incorrect class based on semantic similarity). In our experiments, we consider symmetric noise with noise rates of 20% and 50%, which are **independent of the input features**. Additionally, based on class-wise correlations, we design a 40% asymmetric noise setting on CIFAR-10.
- **CIFAR-10N/100N(Wei et al. 2022)⁴:** These datasets introduce real-world label noise based on standard CIFAR-10 and CIFAR-100. Each image is annotated by multiple human workers, and the final label is obtained via majority voting, thereby reflecting more natural and realistic label noise. Previous studies have shown that **the noise is not independent of the input features**. CIFAR-10N includes five noise levels (Aggregate: 9.03%, Random 1: 17.23%, Random 2: 18.12%, Random 3: 17.64%, Worst: 40.21%), while CIFAR-100N includes one noise level (40.20%).
- **Animal-10N(Song, Kim, and Lee 2019)⁵:** This dataset is constructed based on animal categories from ImageNet. It consists of images from 10 common animal classes collected and labeled by non-expert annotators. The label noise mainly stems from **confusion between**

fine-grained categories, such as dog vs. wolf or cow vs. horse. The estimated noise rate is around 8%.

A more intuitive comparison of the selected datasets is presented in Table E.1.

Dataset	# Class	Noise Type	Noise Ratio
CIFAR	10 / 100	Sym/Asym	20%, 40%, 50%
CIFARN	10 / 100	Real-world	9.03% ~ 40.21%
Animal-10N	10	Real-world	≈8%

Table E.1: Comparison of image datasets

Node Classification. We select three classic citation network datasets: Cora, Citeseer, and Pubmed. In addition, we include the one author collaboration network DBLP for evaluation. To ensure consistency across methods, we randomly sample 20 nodes per class for training. For validation and testing, 500 and 1000 nodes are randomly selected from the graph, respectively. Specifically:

- **Cora, Citeseer and Pubmed (Sen et al. 2008)⁶:** These citation network datasets are widely adopted in graph learning research involving label noise. In each dataset, nodes correspond to academic papers, and edges represent citation connections among them. The node features consist of binary word vectors indicating whether particular words from a vocabulary are present or absent. Each node is labeled according to the research topic category of the corresponding paper.
- **DBLP (Pan et al. 2016)⁷:** This dataset represents an author collaboration network within the field of computer science. Nodes represent documents, while edges correspond to citation relationships between these documents. Node features are derived from word vectors extracted from the text, and labels reflect the category of the research topic.

A more intuitive comparison of the selected datasets is presented in Table E.2.

Dataset	# Class	# Node	# Edge	# Feat.
Cora	7	2,708	5,278	1,433
Citeseer	6	3,327	4,552	3,703
Pubmed	3	19,717	44,324	500
DBLP	4	17,716	52,867	1,639

Table E.2: Comparison of graph datasets

E.2 Baselines

We compare with four categories, 16 baselines in two scenarios: ① Classic IB methods; ② IB with robust loss functions; ③ Improved IB variants; ④ Two-stage denoising + IB methods. They comprehensively evaluate our LaT-IB’s performance from multiple perspectives. Specifically:

⁶<https://github.com/kimiyoung/planetoid/tree/master/data>

⁷<https://github.com/abojchevski/graph2gauss/raw/master/data>

³<https://www.cs.toronto.edu/~kriz/cifar.html>

⁴<https://github.com/UCSC-REAL/cifar-10-100n/tree/main>

⁵<https://dm.kaist.ac.kr/datasets/animal-10n/>

Image Classification.

- Classical IB Models: This paper selects two IB methods, **VIB** (Alemi et al. 2017) and **NIB** (Kolchinsky, Tracey, and Wolpert 2019), as baseline approaches. The core idea of VIB is to approximate the optimization of the IB objective using variational inference. NIB further extends the original IB principle to address the limitations of KL divergence estimation in VIB, which is restricted by the assumptions and simplicity of the prior distribution. Instead of relying on an analytical KL computation, NIB adopts kernel density estimation (KDE) for learning.
- IB with robust loss functions: In the IB framework, the mutual information $I(Z; Y)$ is typically optimized via cross-entropy. The **Generalized Cross-Entropy (GCE)** loss (Zhang and Sabuncu 2018) combines cross-entropy and mean absolute error to enhance robustness. The **Symmetric Cross-Entropy (SCE)** loss (Wang et al. 2019) integrates standard cross-entropy with reverse cross-entropy, improving resistance to label noise. By replacing the original loss with these robust alternatives, new IB variants are constructed under robust loss functions.
- Improved IB Methods: Many subsequent studies have enhanced the feature extraction capability and robustness of IB. The **SIB** (Yang et al. 2025) framework leverages an auxiliary encoder to capture missing structural information, improving learning performance. **DT-JSCC** (Xie et al. 2023) proposes a robust encoding architecture based on the IB principle to improve transmission resilience under varying communication channels. These two methods represent improved IB frameworks and are included in the baseline comparisons.
- Two-Stage Denoise + IB Methods: Although Theorem 3.1 indicates that denoising followed by IB may not yield optimal results, this study further explores this approach. Three representative denoising methods are adopted: **JoCoR** (Wei et al. 2020), a robust learning method based on co-training; **ELR+** (Liu et al. 2020), which uses noise-robust regularization for label correction; and **ProMix** (Xiao et al. 2023), which integrates Mixup data augmentation and dynamic confidence modeling, representing a state-of-the-art denoising approach. These denoised datasets are subsequently used for IB training.

Node Classification.

- Classical IB Models: This paper selects the **GIB** (Wu et al. 2020) method as the classical IB baseline. GIB leverages the IB principle by learning graph representations that compress input feature and structure while preserving label-relevant information.
- IB with robust loss functions: Consistent with the robust loss settings used in the image classification task.
- Improved IB Methods: Two representative improvements are included. **CurvGIB** (Fu et al. 2025) introduces discrete Ricci curvature into the IB framework to better capture topological structures in graphs, enabling the model

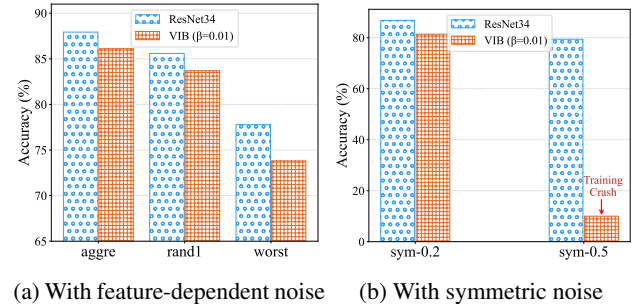
to discard spurious connectivity information and preserve label-relevant substructures. **IS-GIB** (Yang et al. 2023) enhances generalization under distribution shifts by jointly modeling individual and structural information bottlenecks, improving the robustness and transferability of graph representations.

- Two-Stage Denoise + IB Methods: For denoise model, **RNCGLN** (Zhu et al. 2024) first applies graph contrastive learning and multi-head self-attention to learn local-global representations, followed by pseudo-labeling strategies to address graph and label noise. **CGNN** (Yuan et al. 2023) performs neighborhood-based label correction and contrastive learning to smooth representations across graph views. It iteratively corrects noisy labels using neighbors’ predictions before applying the IB objective for final node classification.

E.3 Preliminary Experiment

Vulnerability of IB Methods to Noisy Labels. To investigate the sensitivity of IB methods to label noise, we first conduct preliminary experiments on image classification and node classification to examine the relationship between IB performance and label corruption.

For image classification, Figure E.1a demonstrates that the VIB (Alemi et al. 2017) framework suffers performance degradation on the CIFAR-10N (Wei et al. 2022) dataset as label noise increases. Moreover, the decline becomes more pronounced with higher noise levels. In extreme cases, excessive noise can even lead to training collapse under the IB framework as shown in Figure E.1b.



(a) With feature-dependent noise (b) With symmetric noise

Figure E.1: Preliminary Experiments on Image Classification.

For node classification, Figure E.2a shows that GIB (Wu et al. 2020) gradually fits the noisy labels during training, leading to a steady decline in performance on the testing set. Furthermore, Figure E.2b, using the Cora dataset as an example, illustrates that this trend becomes increasingly severe as the level of label noise increases.

Performance Degradation in Cascaded Models. Theorem 3.1 shows that cascading models weakens the denoising effect of the first stage. This phenomenon is further illustrated in Figure E.3, where the data is first denoised using the ELR+ model and then used to train with the IB method. The resulting performance often falls short of the accuracy achieved after denoising alone.

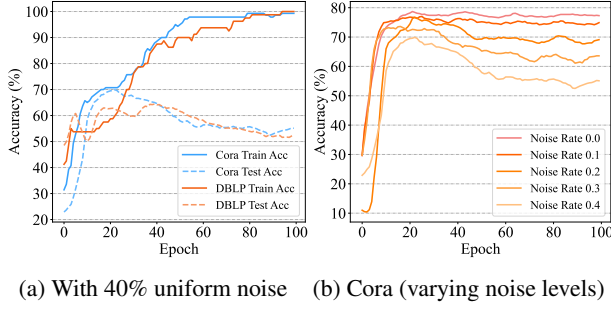


Figure E.2: Preliminary Experiments on Node Classification.

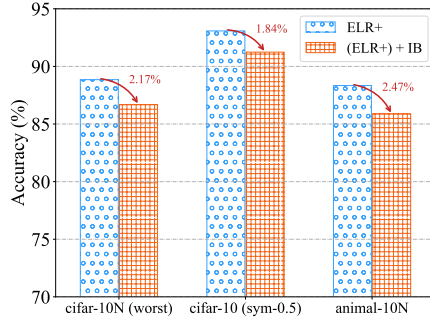


Figure E.3: Performance degradation.

E.4 Additional Results

Table E.3, E.4 and E.5 presents a broader comparison of various LaT-IB methods under different types and levels of noise. We use a dash (-) to denote cases where the model fails or produces invalid results. Classification accuracy (%) is used as the evaluation metric, where a higher value indicates better model performance.

For image classification, the model does not consistently outperform denoise + IB approaches in some cases. A possible explanation is that the denoising models are particularly effective on the CIFAR dataset, thereby significantly enhancing the IB performance. To further validate this, we also evaluated on the Animal-10N dataset, as shown in Table 2, where LaT-IB achieves the best performance. Moreover, Table 4 demonstrates that our method substantially outperforms two-stage approaches under adversarial attacks, further confirming the superiority of LaT-IB.

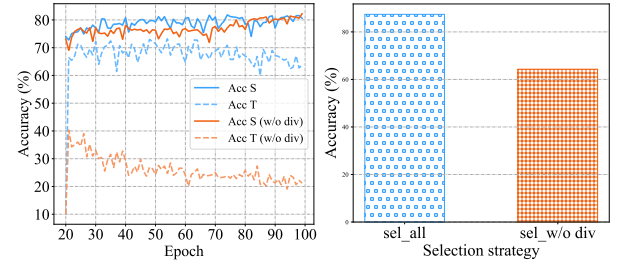
For the node classification task, it is evident that under high noise conditions, our model significantly outperforms other competitive baselines as shown in Table E.4 and E.5, indicating the strong robustness of LaT-IB to label noise.

E.5 Analysis of Sample Selection Strategy

Our proposed sample selection strategy is based on two key components: mutual information and divergence. Mutual information is indirectly measured through the cross-entropy loss, whose effectiveness has been validated in numerous prior works (Arpit et al. 2017; Song et al. 2019). As for

divergence, following Observation 4.2, we adopt Jensen-Shannon (JS) divergence as a criterion to filter samples. This section primarily investigates how divergence affects the learning behavior of the encoder.

Figure E.4a shows the training process during the knowledge injection stage on the CIFAR-10N (worst) dataset, comparing the original method (sel_all) with a variant that excludes divergence-based selection (sel_w/o div). Figure E.4b presents the final performance of both methods. Experimental results demonstrate that removing divergence leads to a larger accuracy gap between the two encoders but ultimately worse performance. We attribute this to encoder T failing to learn meaningful representations of noisy samples, rendering its predictions less informative. As a result, it is unable to provide effective guidance for feature separation in the third stage. These findings confirm that divergence-based sample selection plays a critical role in training the encoder effectively.



(a) Training Process of Knowledge Injection (b) Training Accuracy under Different Selection Strategy.

Figure E.4: The influence of D_{JS}

E.6 Hyperparameter Sensitivity Analysis of δ in Algorithm B.2

In this section, we investigate the effect of the hyperparameter δ , which controls the amount of knowledge the encoder (S, T) acquires during the Knowledge Injection phase. Figure E.5 illustrates the model’s performance on the Cora and Citeseer datasets under various noise types and levels.

The results show that neither excessively high nor low values of δ yield optimal performance. We hypothesize that a too-small δ limits the encoder’s exposure to training data, impairing its ability to learn useful representations. Conversely, a too-large δ causes the two encoders to converge in their learning, reducing their ability to distinguish between clean and noisy information effectively.

Furthermore, the influence of δ varies across datasets, indicating that the model’s capacity to separate clean and noisy information is dataset-dependent.

E.7 Analysis of Model Learning Behavior

To further investigate the learning behavior of the encoder, we perform a t-SNE dimensionality reduction analysis on the embeddings obtained from models trained on the CIFAR-10N (worst) dataset. For a comprehensive comparison, we analyze the embeddings under the following four

Method	Model	CIFAR-10				CIFAR-100	
		20%(sym)	50%(sym)	40%(asym)	20%(sym)	50%(sym)	
Classic IB	VIB	81.49 \pm 1.00	72.58 \pm 1.63	79.27 \pm 1.13	53.86 \pm 0.47	44.25 \pm 0.98	
	NIB	83.44 \pm 0.83	76.16 \pm 1.27	78.16 \pm 1.32	55.99 \pm 0.79	46.20 \pm 0.77	
Robust Loss	VIB (L_{GCE})	88.43 \pm 0.17	84.82 \pm 0.33	81.32 \pm 1.61	—	—	
	VIB (L_{SCE})	84.36 \pm 0.13	77.67 \pm 1.40	76.59 \pm 0.73	53.06 \pm 1.83	—	
Improved IB	SIB	86.40 \pm 0.55	65.52 \pm 1.53	80.06 \pm 1.52	57.64 \pm 1.92	35.01 \pm 1.23	
	DT-JSCC	84.51 \pm 0.41	72.49 \pm 0.77	80.95 \pm 0.41	49.58 \pm 0.13	35.80 \pm 0.96	
Denoise + IB	JoCoR+VIB	88.71 \pm 0.18	81.71 \pm 0.21	60.66 \pm 0.08	62.61 \pm 0.27	53.69 \pm 0.11	
	(ELR+)+VIB	93.16 \pm 0.23	91.28 \pm 0.06	84.75 \pm 0.11	71.44 \pm 0.93	54.12 \pm 0.20	
	Promix+VIB	92.98 \pm 0.14	92.40 \pm 0.10	91.87 \pm 0.05	71.89 \pm 0.16	69.77 \pm 0.56	
Ours	LaT-IB	94.56 \pm 0.12	91.13 \pm 0.16	88.89 \pm 0.73	75.79 \pm 0.19	67.28 \pm 0.55	

Table E.3: Classification accuracy (%) of CIFAR under Symmetric/Asymmetric Noise. All the best results are highlighted in **bold**, and the second-best results are underlined.

Method	Model	Clean	Uniform Noise				Pair Noise			
			10%	20%	30%	40%	10%	20%	30%	40%
ClassicIB	GIB	75.33 \pm 3.19	75.10 \pm 2.48	73.03 \pm 5.67	72.77 \pm 2.36	57.17 \pm 7.83	74.73 \pm 4.39	69.80 \pm 6.18	66.30 \pm 6.60	46.60 \pm 5.45
Robust Loss	GIB (\mathcal{L}_{GCE})	75.03 \pm 2.79	74.43 \pm 3.01	72.03 \pm 6.91	72.27 \pm 4.07	57.57 \pm 6.42	73.67 \pm 3.85	71.03 \pm 4.62	62.60 \pm 6.99	43.63 \pm 6.69
	GIB (\mathcal{L}_{SCE})	74.23 \pm 3.56	72.67 \pm 2.55	71.10 \pm 6.45	70.63 \pm 4.03	58.47 \pm 5.17	73.33 \pm 4.64	70.07 \pm 4.93	59.87 \pm 6.40	43.10 \pm 6.80
Improved IB	CurvGIB	70.67 \pm 3.23	67.67 \pm 2.71	64.63 \pm 6.52	61.97 \pm 4.46	54.47 \pm 6.13	66.93 \pm 1.79	64.03 \pm 4.55	56.27 \pm 7.96	45.03 \pm 1.68
	IS-GIB	54.73 \pm 0.15	53.17 \pm 1.48	42.93 \pm 2.46	45.53 \pm 0.79	38.77 \pm 6.34	49.73 \pm 0.82	46.97 \pm 1.19	40.33 \pm 3.64	38.80 \pm 1.22
Denoise + IB	RNCGLN+GIB	74.70 \pm 2.65	73.37 \pm 0.65	72.97 \pm 5.09	70.80 \pm 2.57	52.27 \pm 6.65	75.00 \pm 3.45	69.93 \pm 3.40	64.67 \pm 6.10	39.83 \pm 7.13
	CGNN+GIB	73.17 \pm 1.86	69.37 \pm 6.01	67.67 \pm 5.28	67.70 \pm 1.85	54.70 \pm 5.06	66.53 \pm 5.74	64.80 \pm 6.16	52.00 \pm 5.40	44.33 \pm 4.74
Ours	LaT-IB	74.57 \pm 0.99	75.87 \pm 0.33	71.13 \pm 2.22	75.60 \pm 0.71	62.53 \pm 7.56	75.43 \pm 1.04	73.70 \pm 3.10	68.57 \pm 3.02	53.00 \pm 7.26

Table E.4: Classification accuracy (%) on the DBLP dataset under different noise types and noise rates. All the best results are highlighted in **bold**, and the second-best results are underlined.

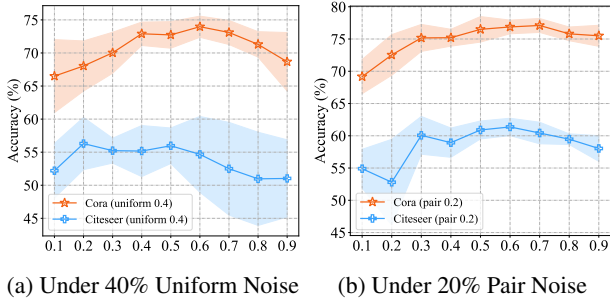
Method	Model	Cora				Citeseer			
		Uniform		Pair		Uniform		Pair	
		20%	40%	20%	40%	20%	40%	20%	40%
ClassicIB	GIB	75.37 \pm 2.47	71.60 \pm 1.51	73.73 \pm 0.39	65.27 \pm 3.84	60.00 \pm 3.37	48.20 \pm 2.20	57.50 \pm 2.35	43.67 \pm 2.90
Robust Loss	GIB (\mathcal{L}_{GCE})	74.77 \pm 0.76	70.47 \pm 2.25	75.00 \pm 1.77	65.27 \pm 2.52	60.20 \pm 3.93	50.80 \pm 2.14	58.73 \pm 2.31	41.03 \pm 1.25
	GIB (\mathcal{L}_{SCE})	74.40 \pm 0.45	69.17 \pm 1.09	<u>75.97</u> \pm 2.02	<u>66.73</u> \pm 4.08	58.83 \pm 5.19	50.93 \pm 0.84	59.10 \pm 3.61	41.40 \pm 1.35
Improved IB	CurvGIB	65.90 \pm 3.69	52.63 \pm 3.23	67.17 \pm 2.11	52.00 \pm 3.19	49.80 \pm 4.19	46.20 \pm 1.69	48.77 \pm 2.09	38.70 \pm 3.70
	IS-GIB	69.20 \pm 0.62	54.73 \pm 1.28	70.30 \pm 0.99	56.47 \pm 4.54	55.73 \pm 3.44	39.03 \pm 1.10	54.90 \pm 4.28	40.13 \pm 2.36
Denoise + IB	RNCGLN+GIB	74.53 \pm 1.58	<u>71.67</u> \pm 1.49	73.57 \pm 1.59	63.60 \pm 3.40	60.90 \pm 2.95	52.83 \pm 4.82	55.77 \pm 3.17	46.00 \pm 3.01
	CGNN+GIB	70.53 \pm 4.69	64.73 \pm 6.75	73.57 \pm 1.37	59.00 \pm 3.29	57.53 \pm 3.73	45.73 \pm 4.29	54.43 \pm 3.30	41.57 \pm 1.90
Ours	LaT-IB	74.30 \pm 2.01	74.07 \pm 1.46	76.87 \pm 1.06	66.80 \pm 3.14	61.63 \pm 2.24	55.17 \pm 3.86	58.93 \pm 2.77	46.00 \pm 0.71

Table E.5: Classification accuracy (%) on the Cora and Citeseer dataset under different noise types and noise rates. All the best results are highlighted in **bold**, and the second-best results are underlined.

settings: ① VIB without the $I(X; Z)$ constraint, which is approximately equivalent to a standard ResNet34 model; ② Standard VIB model; ③ LaT-IB model at the end of Knowledge Injection, referred to as LaT-IB KI; ④ Full LaT-

IB model.

Figure E.6a and E.6b show that IB methods produce more compact embeddings by minimizing $I(X; Z)$, reducing the encoding space and slightly lowering performance. Figure



(a) Under 40% Uniform Noise (b) Under 20% Pair Noise

Figure E.5: The influence of δ

E.6c and E.6d illustrate that the third robust training stage of LaT-IB further restricts $I(\mathcal{D}; S, T)$ and improves noise robustness. In particular, Figure E.6d shows embeddings **similar to IB's minimal sufficient property** (Figure E.6b), while clearer class boundaries demonstrate LaT-IB's ability to **learn cleaner representations**.

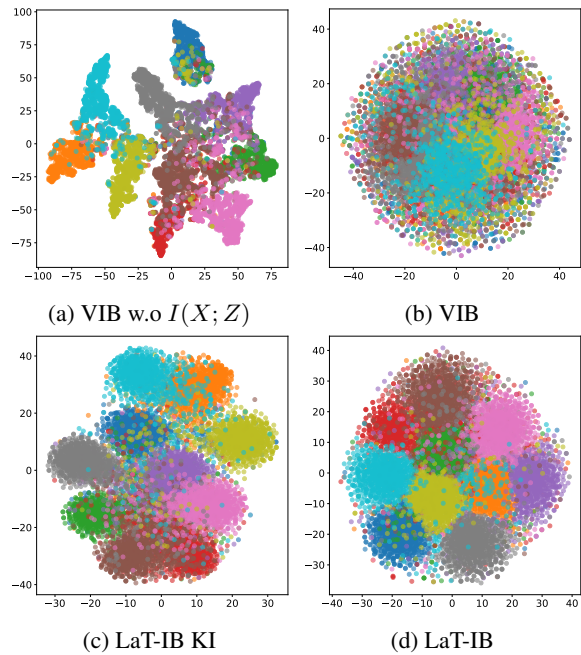


Figure E.6: The embedding distributions of different models

To investigate the learning process of the two encoders S and T , Figure E.7 shows their prediction accuracy on training and test sets with 40% uniform noise on the Cora dataset, where vertical dashed lines divide the process into three periods. Encoder T gradually fits all (noisy) data, while S , influenced by T , achieves about 65% accuracy on the training set by fitting **mostly clean data**.

E.8 Hyperparameter settings

Image Classification. For CIFAR-related datasets, we set the batch size to 256, and each image is reshaped to a size of (32, 32). For the Animal-10N dataset, the batch size is set

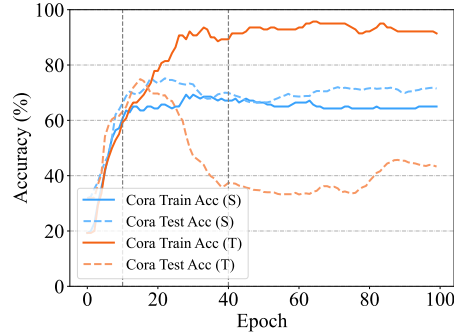


Figure E.7: The learning behavior of (S, T)

to 128, and each image is reshaped to (68, 68). We use SGD as the optimizer with a learning rate of 0.005, momentum of 0.9, and a weight decay of 5e-4. A cosine learning rate scheduler is applied.

The dimension of the encoder's latent space is set to 128. Each experiment is repeated three times, and we report the mean and standard deviation of the results.

Node Classification. For node classification tasks, we use the Adam optimizer with a learning rate of 0.001. To enable the computation of structural KL divergence, the model backbone is configured as a two-layer GAT. In our hyperparameter settings, the KL divergence weight for the features is set to 0.001, and the weight for the structural KL divergence is set to 0.01. The dimension of the encoder's latent space is set to 16 or 20. Each experiment is repeated three times, and we report the mean and standard deviation of the results.

In the experiments, the Algorithm B.2 uses $\delta \in \{0.1, 0.2, \dots, 0.9\}$. Besides, we set $\beta \in \{1e^{-1}, \dots, 1e^{-5}\}$ and $\gamma \in \{1e^0, \dots, 1e^{-4}\}$ in our hyperparameter configuration. The predicted confidence scores are set based on the learning behavior of Warmup samples for each dataset, ensuring that the upper confidence bound is greater than 0.5, while the lower confidence bound is less than 0.5.

E.9 Hardware and Software Configurations

We conduct the experiments with:

- Operating System: Ubuntu 22.04.4 LTS.
- CPU: Intel(R) Xeon(R) Silver 4110 CPU @ 2.10GHz.
- GPU: NVIDIA Tesla V100 SMX2 with 32GB of Memory.
- Software: CUDA 12.8, Python 3.10.12, PyTorch⁸ 2.2.0, PyTorch Geometric⁹ 2.6.1.

⁸<https://github.com/pytorch/pytorch>

⁹https://github.com/pyg-team/pytorch_geometric